Nano Research

ISSN 1998-0124 CN 11-5974/O4
https://doi.org/10.26599/NR.2026.94908759

Research Article

3D bioprinting of hepatocyte-derived exosome-reinforced skin organoid for efficient skin regeneration

Bhavana Rajbanshi[1], Churong Xu[3], Surendra Shrestha[5], Ruihan Hao[3], Yuxin Qi[3], Zhouyi Duan[3], Ding Ma[3], Qichen Li[3], Fangzheng Cheng[3], Liming Dai[3], Miao Jiang[1](✉), Xiaoling Zhang[3](✉), Bingjun Zhang[4](✉), Jingjun Zhao[1,2](✉)

[1] Department of Dermatology and Venereology, Tongji Hospital,School of Medicine, Tongji University, Shanghai 200092, China

[2] Department of Dermatology, Xinhua Hospital Affiliated to Shanghai Jiao Tong University School of Medicine, Shanghai 200092, China

[3] Department of Orthopedics, Xinhua Hospital Affiliated to Shanghai Jiao Tong University School of Medicine, Shanghai 200092, China

[4] Suzhou Institute of Biomedical Engineering and Technology, Chinese Academy of Sciences, Suzhou 215163, China

[5] Department of Pediatrics, Maria Fareri Children's Hospital at Westchester Medical Center, Valhalla, NY 10595, USA

Nano Res., **Just Accepted Manuscript** • https://doi.org/10.26599/NR.2026.94908759

https://www.sciopen.com/journal/1998-0124 on Apr. 20, 2026

Research Article

3D bioprinting of hepatocyte-derived exosome-reinforced skin organoid for efficient skin regeneration

Bhavana Rajbanshi[1], Churong Xu[3], Surendra Shrestha[5], Ruihan Hao[3], Yuxin Qi[3], Zhouyi Duan[3], Ding Ma[3], Qichen Li[3], Fangzheng Cheng[3], Liming Dai[3], Miao Jiang[1], Xiaoling Zhang[3*], Bingjun Zhang[4*], and Jingjun Zhao[1,2*]*

1. Department of Dermatology and Venereology, Tongji Hospital, School of Medicine, Tongji University, Shanghai 200092, China
2. Department of Dermatology, Xinhua Hospital Affiliated to Shanghai Jiao Tong University School of Medicine, Shanghai 200092, China
3. Department of Orthopedics, Xinhua Hospital Affiliated to Shanghai Jiao Tong University School of Medicine, Shanghai 200092, China
4. Suzhou Institute of Biomedical Engineering and Technology, Chinese Academy of Sciences, Suzhou 215163, China
5. Department of Pediatrics, Maria Fareri Children's Hospital at Westchester Medical Center, Valhalla, NY 10595, USA

Received: 23 February 2026; **Revised:** 19 April 2026; **Accepted:** 20 April 2026

Address correspondence to Jingjun Zhao, zhaojingjun2015@aliyun.com; Bingjun Zhang, smior122@163.com; Xiaoling Zhang, xlzhang@shsmu.edu.cn; Miao Jiang, jiang-miao@126.com

Cite this article: *Nano Research*, 2026, 19, 94908759 https://doi.org/10.26599/NR.2026.94908759

Abstract

Third-degree, large-area skin injuries impose a significant socioeconomic burden on victims each year. The liver demonstrates extensive regenerative properties, and its exosomes are rich in organic selenium protein (SELENOP) with a high bioavailability. In this study, given its unique cargo, we established hepatic exosomes as a distinct biological nanoparticle to investigate their regenerative effects on skin cells, including upregulation of cell growth, antioxidant molecules, and angiogenic properties, which have not been previously explored. Building on these promising findings, we designed a novel 3D (three-dimensional) bio-printed multicellular skin

organoid scaffold using hepatic exosome-encapsulated GECM (GelMa-ECM) bio-ink to mimic native skin structure. In vivo, the skin construct orchestrates wound healing by boosting key tissue regenerative markers, biological processes, and signaling pathways, while also downregulating various pro-inflammatory pathways during the proliferative stage of healing. Our study highlights a new strategy for wound healing and offers potential insights into the treatment of other chronic and recalcitrant skin diseases.

Keywords: skin organoid, hepatocyte-derived exosomes, three-dimensional (3D) printing, wound regeneration

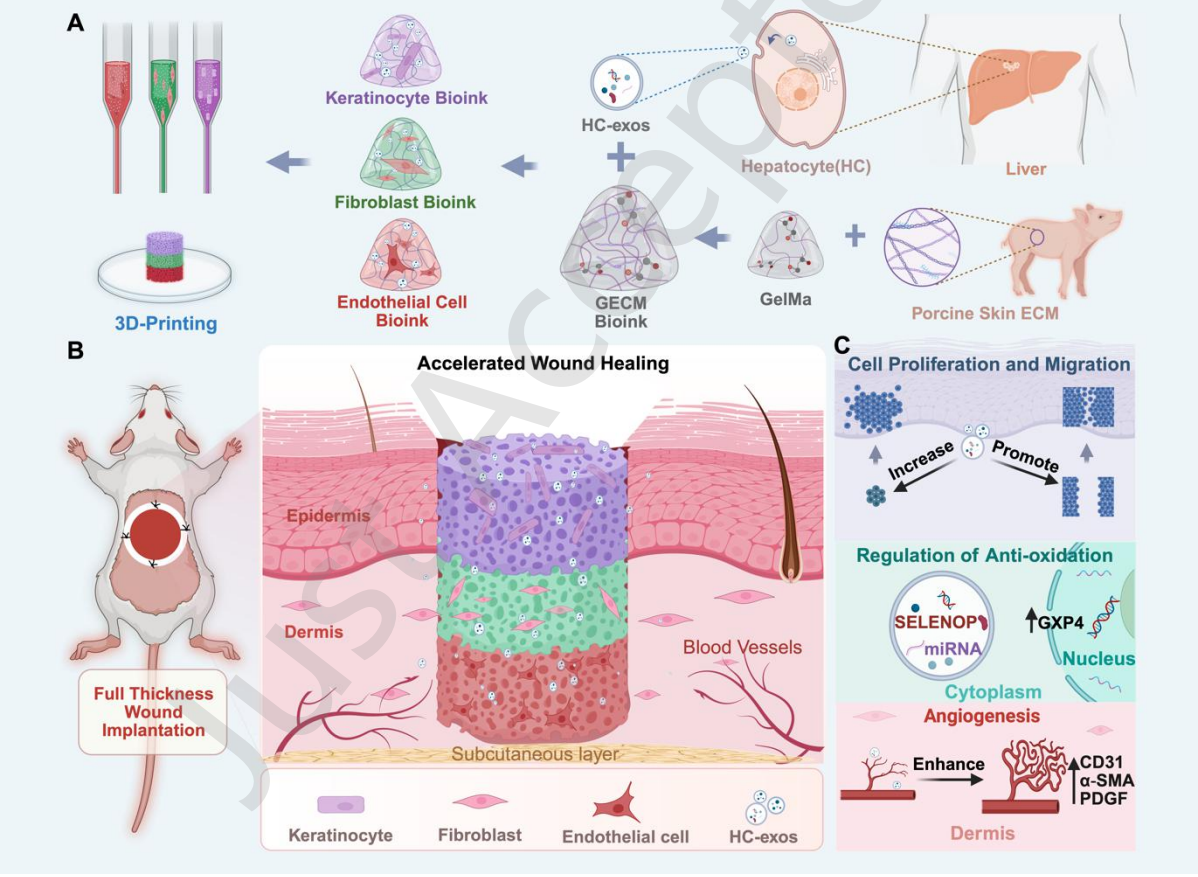

Fig. 1. Schematic illustration of the design and bio-printing of a skin organoid for wound healing, featuring a multicellular spatial distribution structure using hepatic cell-derived exosomes (HC-exos) encapsulated bio-ink. A) Preparation of bio-ink for printing of skin microtissue. B) Transplantation of the viable scaffold in a full-thickness wound animal model. C) Cellular and molecular mechanisms induced by the skin organoid in promotion of wound healing

through the modulation of signaling pathways, key genes, and protein expression, and angiogenesis.

1. Introduction

Skin healing is a complex, dynamic process involving various cell types within the skin and other organs through their secretome, including proteins, exosomes, metabolites, and more, contributing to biological processes like proliferation, angiogenesis, and genetic regulation[1-3]. It primarily occurs in four phases: hemostasis, inflammation, proliferation, and remodeling. Third-degree large-area skin wounds, which are more prone to necrosis and cannot be sutured, caused by thermal injuries, trauma, and surgical procedures, impose a significant socioeconomic burden on patients and compromise their quality of life[4]. Although autologous skin grafts are the gold standard treatment for such injuries, limited graft sources and graft failure due to infection or inadequate perfusion remain challenging[5]. Therefore, there is an urgent need for alternatives to skin grafts that can heal complex wounds requiring extended recovery periods. Besides the difficulties in healing these wounds, the formation of hypertrophic scars remains inherently challenging.

3D (three-dimensional) printing technology can facilitate the creation of organoid scaffolds with the flexibility to replicate the spatiotemporal coordination among different cell types more precisely and on a large scale[6]. These models are also essential for studying the dynamic behavior of cells in a 3D environment resembling the complex microenvironment of the human body, and contribute to providing advanced biological insights for treating complex wounds over the long term. By maneuvering this technology, researchers have fabricated normal and pathological 3D skin models and conducted drug testing, which has significant implications for clinical translation[7-9]. Orthotopic implantation of such skin organoids is emerging as a promising approach in skin regeneration, providing bio-mimicking tissue that promotes efficient regeneration by regulating the healing microenvironment[10]. However, clearance of cells within the scaffold by activated immune cells and excessive ROS (reactive oxygen species) may hinder the repair process. Thus, recent research emphasizes integrating exosomes from various sources,

considering their unique cargo, to strengthen cells within the construct and improve their regenerative efficiency for skin and other tissues[11-13].

The liver plays a critical role in maintaining homeostasis and has extensive regenerative capacity, even after 70% of the liver has been removed[14]. Exosomes released from healthy liver cells are crucial for the organ regeneration, mainly through the synthesis of sphingosine-1-phosphate (S1P), a vital sphingolipid involved in cellular proliferation, motility, immune regulation, and vascular development[15, 16]. The liver is the only organ responsible for assembling absorbed essential trace element selenium (Se), and metabolizing it into selenium protein (SELENOP), which are also transported via exosomes to different organs of our body. This is critical for maintaining homeostasis, boosting immune response, upregulating potent antioxidant enzymes, and exerting anti-cancer activity[17-19]. Due to Se's beneficial effects in supporting various biological functions, efforts have been made to improve the delivery of synthesized Se nanoparticles to treat atopic dermatitis, androgenetic alopecia, and to support skin and bone healing[20-22]. However, concerns about the toxicity of high concentrations of inorganic Se nanoparticles and their low bioavailability persists. Researchers have also identified various chronic dermatological diseases, such as prurigo nodularis and psoriasis, which are linked to liver pathologies through the 'Liver-Skin' axis[23-25]. Nevertheless, the regenerative effects of exosomes from normal liver tissue on skin cells are yet to be investigated.

Inspired by the liver's remarkable regenerative capacity and hepatic exosomes carrying organic Se with high bioavailability, we explored regenerative properties on the three types of skin cells induced by the exosomes. Post-treatment the cells showed improved regenerative function and higher expression of potent antioxidants like glutathione peroxidase. Subsequently, we engineered a novel 3D printed skin organoid scaffold as shown in Fig. 1. The design incorporated the three skin types individually with GelMa-ECM bio-ink empowered by hepatic exosomes. After layer-by-layer extrusion-based bioprinting, it was photo-cured to mimic skin microanatomy. While testing its effectiveness and molecular mechanisms in vivo, the organoid demonstrated remarkable proliferative, angiogenic, and antioxidant effects, enhancing the wound healing microenvironment. Our findings also highlight its potential in scar remodeling through accelerated transition of Collagen III to Collagen I. Due to its high biocompatibility, efficacy,

and adaptability, this innovative skin organoid holds significant promise for clinical translation. Our study is a pioneer in exploring the impact of hepatic exosomes on skin regeneration, and our findings could open new avenues for future research on advancing treatments for more complex wounds and dermatological conditions.

2. Results and Discussion

2.1 Effects of conditioned medium and exosomes from hepatocytes on skin cells

There is organ-to-organ cross-talk via secretome released from the normal liver to maintain hemostasis or from an abnormal liver to initiate inflammatory conditions such as psoriasis, rheumatoid arthritis, and inflammatory bowel disease [24-27]. However, it cannot be ignored that the liver is the only organ with an unlimited ability to regenerate[14]. Due to such powerful regenerative capacity, the effects of a normal liver on skin regeneration are of interest. Literature has reported "Liver-Skin" axis elaborating chronic skin conditions such as prurigo nodularis and psoriasis related to liver pathologies [24, 25]. However, effects of normal liver on regeneration of skin remain unknown. Therefore, we explored whether secretome released from hepatic cells could modulate cellular functions essential for tissue regeneration, such as proliferation, migration, and angiogenesis. Conditioned medium (CM), the supernatant from hepatic cells, was added to cultured skin cells, with normal culture-treated skin cells serving as a control, as shown in Fig. S1a. The proliferative effect of CM was tested using a cell counting kit (CCK-8), which showed a significant increase in cell numbers on Day 1, Day 3, and Day 5 for fibroblasts. However, keratinocytes and endothelial cells exhibited a significant increase in proliferation on Day 5 and Day 3, respectively (Fig. S1b-d). Additionally, gene expression regulation in cells after culturing with CM was evaluated through real-time PCR (RT-PCR). Keratinocytes treated with CM showed high expression of Cytokeratin 5 (K5, a basal cell marker) (Fig. S2a), while the expression of Integrin B (IGBT, a marker of cell adhesion and signaling) was not significantly changed (Fig. S2b). Similarly, the expression of genes such as type I collagen-A (COL1A1, essential for collagen formation) and fibronectin (FN, involved in cell adhesion and migration) was significantly increased in treated fibroblasts compared to controls (Fig. S2c, d). Likewise, the CM increased the gene expression of endothelial nitric oxide synthase (eNOS), which is vital

for angiogenesis and vascular homeostasis, and platelet-derived growth factor (PDGF), which is crucial for angiogenesis, proliferation, and vascular remodeling during wound healing and tissue repair (Fig. S2e, f). Furthermore, the angiogenesis assay indicated that CM promoted faster angiogenesis, with a significant increase in the number of nodes, segments, and tube length (Fig. S3a-d).

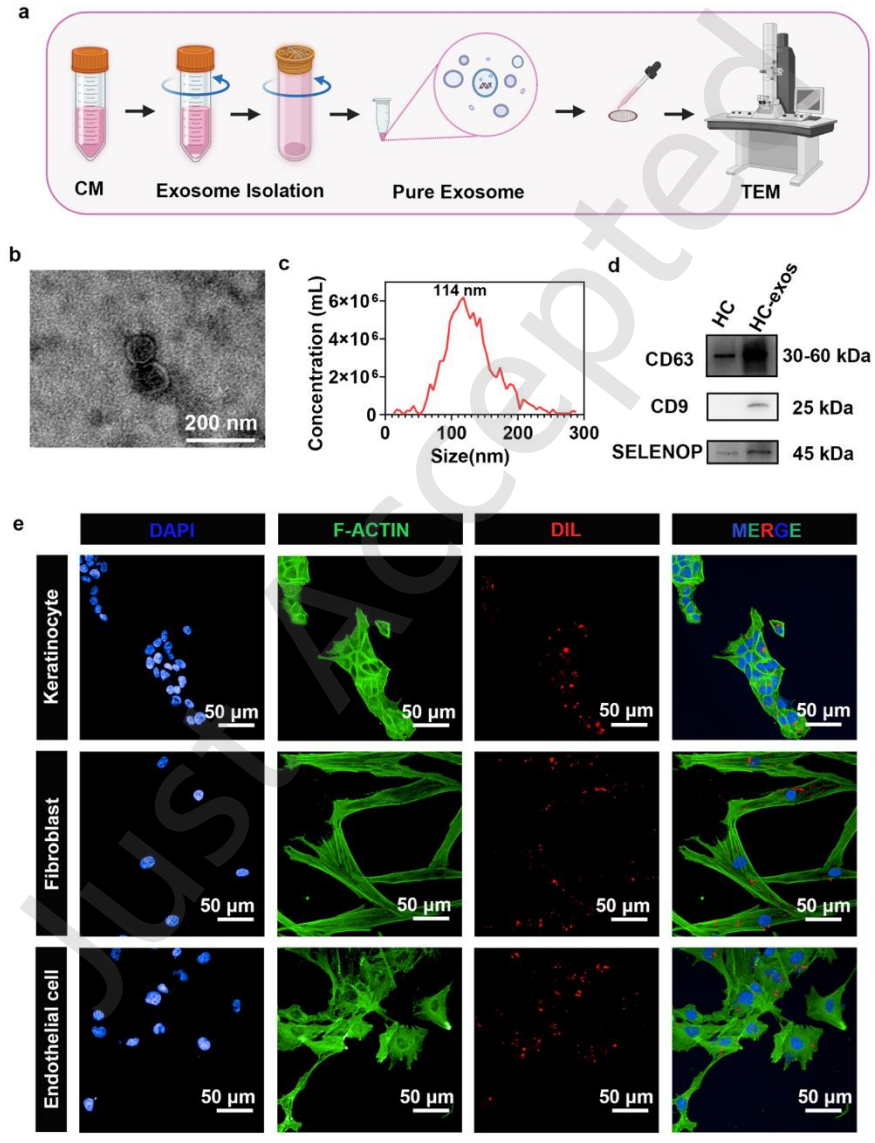

Fig. 2. Characterization of hepatic cell-released exosomes (HC-exos) and their uptake by skin cells. a) Schematic diagram of the exosome isolation procedure. b) Morphology of HC-exos visualized under transmission electron microscope (TEM, scale bar, 200 nm). c) Particle size

distribution via NTA. d) Characteristic exosome surface markers CD63 and CD9, and SELENOP by western blotting. e) Internalization of DIL-labelled HC-exos by keratinocytes, fibroblasts and endothelial cells after 24 hours of incubation, as assessed by fluorescence. Red, blue, and green signals represented HC-exos, nucleus, and cytoskeletal protein, respectively (scale bar, 50 μm).

Exosomes are crucial nano-particles in the secretome released by any cell and play a significant role in intercellular and inter-organ communication. This nano-biomaterial have been studied for decades owing to their cargo-mediated bioactivity, enabling diverse functions such maintain normal physiological functions, including proliferation, differentiation, and genetic regulation[28]. Considering their stability and bioavailability, researchers harnessed them as a carrier for the delivery of proteins, medications, etc[29, 30]. Similarly, hepatic cell-derived exosomes (HC-exos) have been reported to exhibit regeneration and repair of hepatocytes via activation of the sphingolipid pathway for the generation of S1P intracellularly, which is essential in regulating proliferation and migration of various cells[16, 31]. Furthermore, it is protective to neurons and endothelial cells via delivery of a potent SELENOP, which is reported to possess anti-oxidant, anti-inflammatory and cytoprotective effects[19, 32, 33]. Based on the significant impact of CM from hepatocytes on skin cells (Fig. S1-3), we hypothesize that exosomes also have beneficial effects on the skin cells. Hence, as depicted in Fig. 2a, HC-exos were isolated and purified from the CM of hepatic cells. Then, their morphology, size, and surface protein markers were characterized. As shown in Fig. 2b, HC-exos when subjected to transmission electron microscopy (TEM) after negative staining, showed a round double-layered cup-saucer-shaped structure. Particle size of the exosomes was encountered at a range of 50 nm to 250 nm via nano-particle tracking analysis (NTA) with peak concentration 6×10^6 particles/mL and average hydrodynamic diameter 114 nm (Fig. 2c). Upon performing a Western blot, exosome surface markers like CD63 and CD9 were expressed, along with SELENOP (Fig. 2d, S3). These experiments verify the successful isolation of pure HC-exos and presence of SELENOP within. Upon culturing the skin cells with DIL-labelled HC-exos, fluorescence imaging showed exosomal endocytosis by keratinocytes, fibroblasts and endothelial cells within 24 hours (Fig. 2e). These findings suggested that HCs-exos could be successfully internalized by the skin cells.

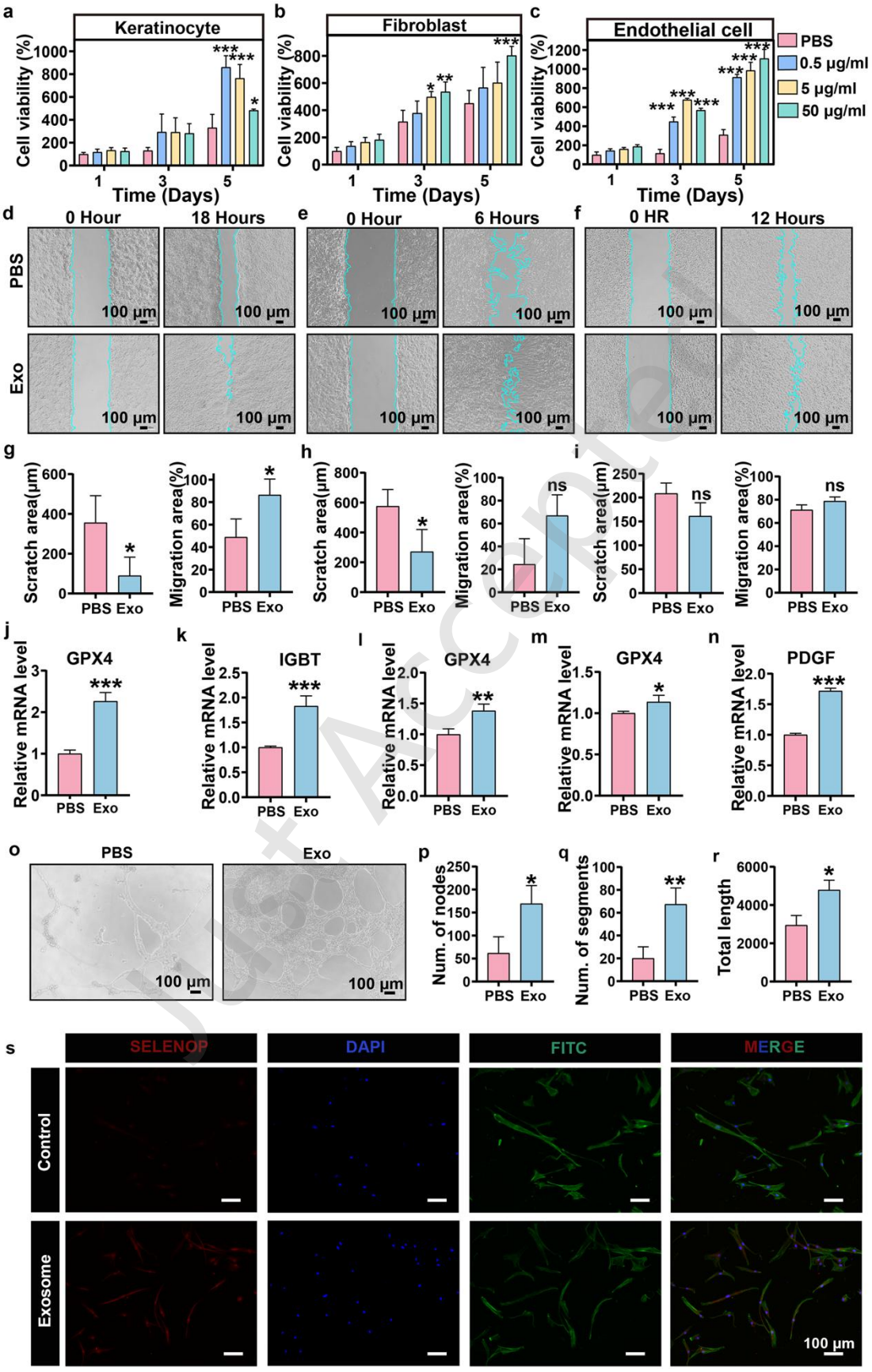

Fig.3. Biological effects of HC-exos on skin cells in a 2D environment. Cell proliferation of a) keratinocytes, b) fibroblasts, and c) endothelial cells cultured with different concentrations of HC-exos on Day 1, Day 3, and Day 5, respectively (n = 3). Cell scratch assay of HC-exos treated d) keratinocytes for 18 hours, e) fibroblasts for 6 hours, and f) endothelial cells for 12 hours (scale bar, 100 μm). Quantitative analysis of cell scratch assay of g) keratinocytes, h) fibroblasts, and i) endothelial cells (n = 3). Relative mRNA expression of j,l,m) GPX4 in all three skin cells, k) IGBT in keratinocytes and n) PDGF in endothelial cells induced by HC-exos treatment verified by RT-qPCR (n = 9). o) Angiogenesis of endothelial cells cultured with HC-exos (scale bar, 100 μm), p-r) Quantitative analysis of the number of nodes, segments, and total length from angiogenesis assay (n = 4). Data reported was mean ± standard deviation (*,$p \leq 0.05$; **,$p \leq 0.01$; ***,$p \leq 0.001$ vs. PBS, ns: not statistically significant). s) Immuno-fluorescence imaging of SELENOP (red), DAPI (blue), and FITC (green) after treatment with HC-exos.

2.2 Repairing potential of the hepatic exosomes on the skin cells

To further confirm whether HC-exos were able to exert the regenerative effects as hepatic secretome on the skin cells, the purified exosomes of different concentrations, namely 0.5 μg ml^{-1}, 5 μg ml^{-1}, and 50 μg ml^{-1}, were added to keratinocytes, fibroblasts, and endothelial cells as the experimental groups with PBS as the control group. The results of cell viability analysis indicated that regardless of any concentration, the HC-exos were highly biocompatible and non-toxic. On day 5, 50 μg ml^{-1} of HC-exos demonstrated a significant promotion in cell viability and proliferation rate on all three skin cells compared to the control (Fig. 3a-c). Hence, we chose it as an optimal concentration for further analysis. The exosomes also demonstrated a significantly superior migratory effect on keratinocytes and fibroblasts, both qualitatively and quantitatively (Fig. 3d-i). Glutathione peroxidase 4 (GXP 4), a potent antioxidant enzyme, facilitates ferroptosis inhibition, eventually mediating tissue regeneration[34]. Upon performing RT-PCR analysis, genetic expression of GXP 4 for HC-exos group demonstrated a significant upregulation in all the skin cells relative to the control (Fig. 3j-n). Concurrently, the genes closely associated with cellular regeneration, including ITGB and PDGF, exhibited markedly increased expression trends in keratinocyte and endothelial cells, respectively (Fig. 3j-n).

Through angiogenesis, neo-vascularization occurs for the perfusion of nutrition and oxygen in the wound region for regeneration. The angiogenesis assay confirmed that HC-exos significantly enhanced endothelial cells' proangiogenic activity (Fig. 3o-r). Further immunofluorescence analysis revealed that after 24-hour co-culture with HC-exos, fibroblasts demonstrated a marked elevation in intracellular SELENOP (Fig. 3s). As a key regulator of selenium metabolism, SELENOP's core function is to support anti-inflammation and anti-oxidation via GPX, providing a molecular basis for subsequent wound healing[32, 33, 35]. In summary, HC-exos can positively alter regenerative properties of skin cells via proliferation, migration, and genetic modulation of key genes and proteins, optimizing regenerative properties. Furthermore, it can also enhance angiogenetic properties in endothelial cells, exerting dual regulatory effects on wound healing.

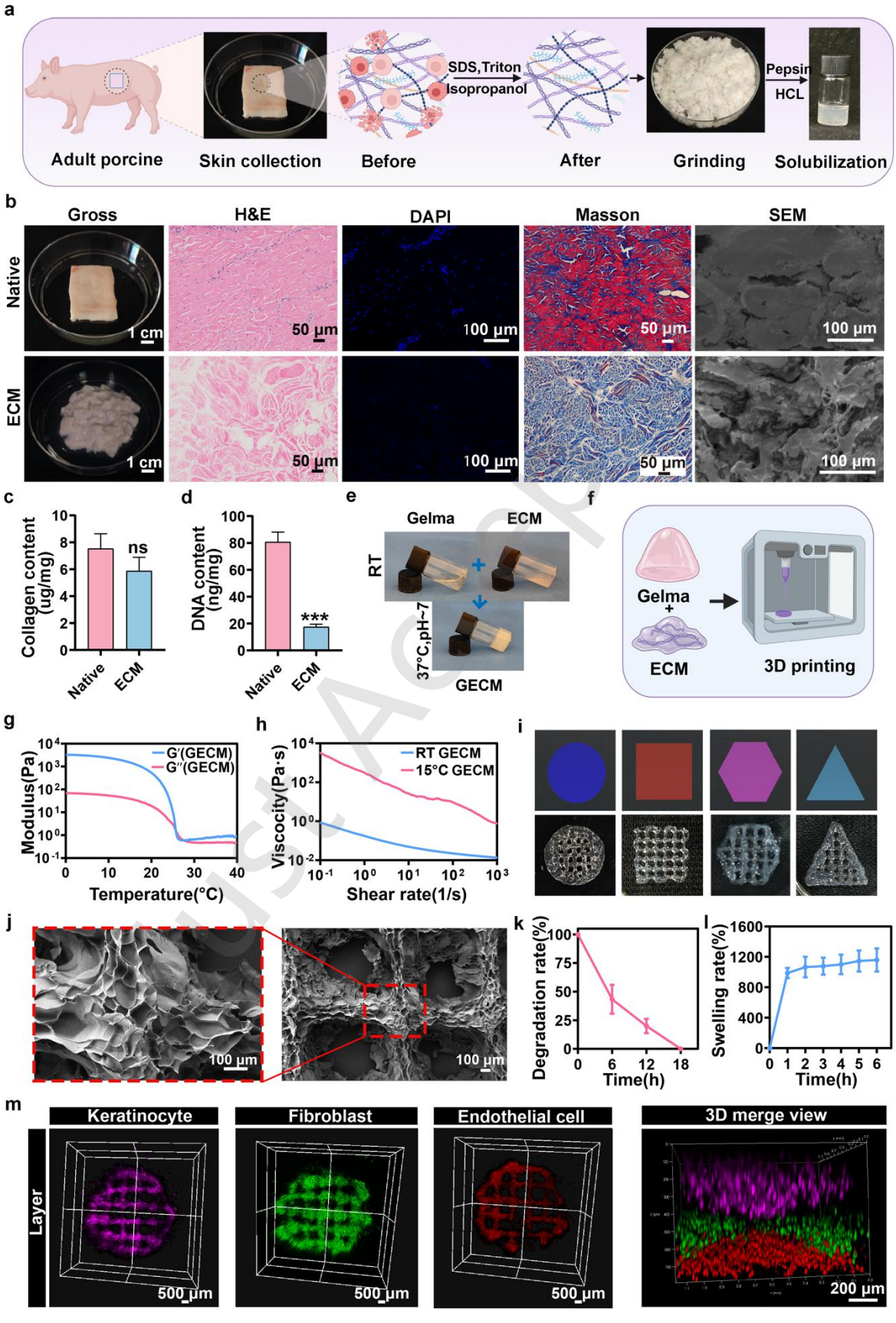

Fig.4. Characterization of bio-ink and fabrication of 3D bio-printed organoid scaffold. a) Diagrammatic illustration of the process of decellularization of native porcine skin. b) Gross view (scale bar, 1cm) and histological analysis of native skin and ECM with H&E staining (scale bar, 50 μm), DAPI (scale bar, 100 μm), Masson Trichome's staining (scale bar, 50 μm), and scanning electron microscopy (SEM, scale bar, 100 μm). Quantitative analysis of c) collagen content (n = 3), and d) DNA content (n = 3) of the tissue before and after decellularization. Data reported was mean ± standard deviation (*,$p \leq 0.05$; **,$p \leq 0.01$; ***,$p \leq 0.001$, ns: not statistically significant). e) The solution-gel phase transition process of the bio-ink composed of ECM and Gelma (GECM) from room temperature (RT) to 37 °C and pH ≈ 7. f) Schematic representation of printing of GECM. g) Dynamic curves of the storage modulus (G') and loss modulus (G'') of GECM. h) Shear thinning behavior of bio ink with shear rate increasing from 0.1 s^{-1} to 10^4 s^{-1}. i) Versatile printability of the scaffold into different shapes. j) SEM images of printed scaffold (scale bar, 100 μm). k) Degradation of the scaffold in 0.5 mg ml^{-1} collagenase when shaken at 37 °C (n = 4). l) Swelling rate of scaffold immersed in PBS at 37 °C (n = 6). m) Spatial observation of 3D printed skin organoid with purple representing keratinocyte layer, green for fibroblast, and red for endothelial layer, followed by three-dimensional (3D) merge view under confocal laser scanning microscope (CLSM, scale bar, 500 μm and 200 μm, respectively).

2.3 Characterization of bio-ink and engineering of 3D printed skin organoid

The extracellular matrix (ECM) is an important component of connective tissue and many organs, responsible for providing physical confinement for growth and communication between the cells[36]. As ECM components derived from porcine skin are highly similar to those of human tissues, tissue-specific ink raw materials were prepared through the decellularization as shown in Fig. 4a. Inefficient decellularization may result in an acute rejection reaction during in vivo implantation. Hence, its efficiency and preservance of collagen were visualized using Hematoxylin and Eosin (HE) and Masson's trichrome staining showing clearance of the cells from the native tissue. Similarly, 4,6-diamidino-2-phenylindole (DAPI) staining further confirmed the elimination of cells in the tissue after decellularization (Fig. 4b). When photographed by a scanning electron microscope (SEM) before decellularization, the tissue

appeared very compact but after decellularization, it became loose, porous, and fibrous (Fig. 4b). The process decreased the collagen content in the ECM; however, the difference compared with native tissue was not significant (Fig. 4c), indicating no significant loss of collagen after the processing. Similarly, quantification of deoxyribonucleic acid (DNA) confirmed the DNA content of the sample to be approximately 16 ng mg^{-1} dry mass (Fig. 4d). These findings confirmed efficient decellularization and a significant decrease in DNA content in the tissue without a significant disruption of the collagen. After adjusting the pH of the liquified ECM to approximately 7 and balancing ions concentration, it exhibited a sol-to-gel transition at 37 °C, verifying its suitability for employing as a component of our bio-ink for printing (Fig. 4e).

ECM solubilized at a concentration of 10 mg ml^{-1} was mixed with 6 % gelatin methyl-anhydride (Gelma) to explore the printability of the hybrid bio-ink GECM (Fig. 4f). Complex modulus analysis revealed, when the temperature rises above 25 °C, bioink's storage modulus drops lower than corresponding loss modulus until 27 °C, which indicates its gel-solution transition. However, with increasing temperature, the storage modulus exceeds the loss modulus resulting in re-gelation highlighting GECM's excellent printability and structural integrity compatible for transplantation in physiological body temperature (Fig. 4g). In addition, the viscosity of the bio-ink was measured which showed that as the shear rate increased from 0.1 to 100 s^{-1}, viscosity decreased significantly, supporting its shear-thinning property. This characteristic is essential for extrusion-based bioprinting as low shear stress during the extrusion is conducive to cell survival (Fig. 4h). To explore the toxicity of the hybrid ink on skin cells, bioink encapsulating different skin cells when subjected to sterile extrusion-based 3D bioprinting into a scaffold and incubated at 37 °C. On Day 1, Day 3, and Day 7, the cells showed good proliferation within the scaffold when stained by Calcein (Fig. S5) which verified biocompatibility of GECM ink for bioprinting. Meanwhile, the GECM demonstrated excellent printing and forming properties, enabling the construction of the scaffolds in various shapes essential for printing of the analogues to match diverse wounds (Fig. 4i). Furthermore, the interior of the hydrogel possessed a distinct large-pore structure when viewed under SEM, which is conducive to cell adhesion and growth. (Fig. 4j). It gradually degraded over time within 18 hours when incubated with collagenase at 37 °C (Fig. 4k) proving it suitable for proper tissue formation. The lyophilized scaffold could swell up to 900 % in one hour and sustain the volume for up to 6 hours, which is essential for the 3D construct to

absorb the culture medium for the nourishment of encapsulated cells (Fig. 4l). Inspired by microanatomy and stratified characteristics of the skin; keratinocytes, fibroblasts and endothelial cells combined with GECM was used to prepare and design the in vitro 3D printed skin organoid (Org). To characterize three types of cells within the organoid, different fluorescent dyes were used to stain three types of cells respectively. The purple fluorescent-labeled keratinocytes, the green fluorescent-labeled fibroblast and the red fluorescent-labeled endothelial cells were respectively distributed in upper, middle and lower layers when observed under a confocal laser microscope (CLMS) (Fig. 4m, S6).

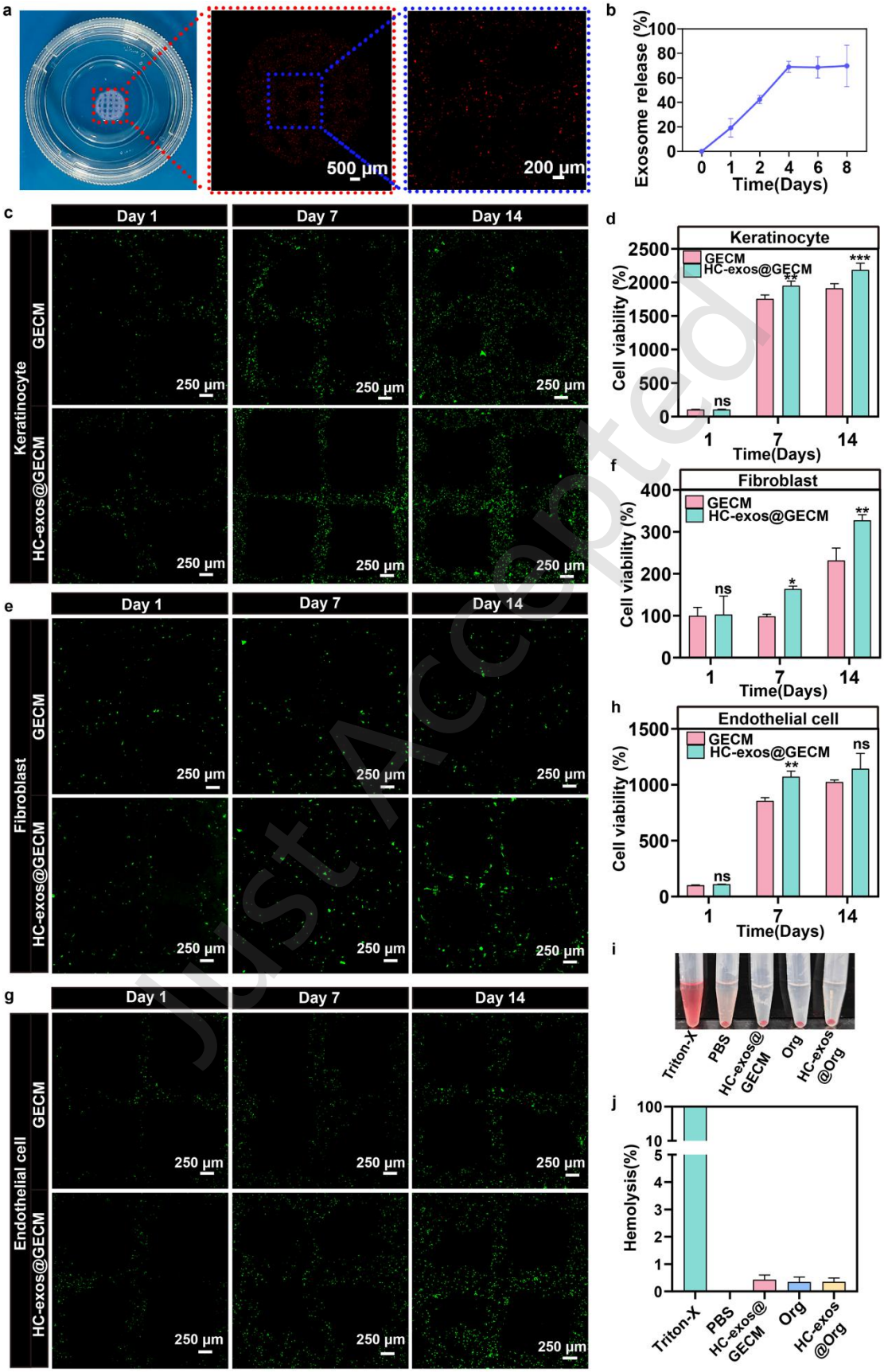

Fig. 5. Regulatory effects of HC-exos encapsulated bio-ink on the skin cells. a) Visual and CLMS observation of the scaffold printed with DIL labelled HC-exos containing bio-ink (scale bar, 500 μm and 200 μm respectively). b) Exosome release assay (n = 3). Calcein staining fluorescence images of c) keratinocytes, e) fibroblast, and g) endothelial cells within GECM scaffolds with or without HC-exos cultured until Day 1, Day 7, and Day 14 (brightness has been adjusted across the images for qualitative visualization) and d,f,h) Cell proliferation rate for the three skin cells within the construct, respectively (n = 3). Data reported was mean ± standard deviation (*,$p \leq 0.05$; **,$p \leq 0.01$; ***,$p \leq 0.001$, ns: not statistically significant). i,j) Hemolysis analysis of extracts from, HC-exos@GECM, Org and HC-exos@Org with Triton-X and PBS set as control (n = 4).

Dioctadecyl-tetramethylindocarbocyanine perchlorate (DIL) labeled HC-exos were then mixed with the GECM and printed into a scaffold. When viewed under a CLSM, the distribution of the exosomes within the scaffold was homogeneous throughout (Fig. 5a). Similarly, the scaffold exhibited a gradual increase in exosome release, reaching a stable release after Day 4 and onwards (Fig. 5b). Cells progressively grew within the 3D bio-printed scaffold, and the exosomes are simultaneously released from the scaffold in a controlled manner. Backed by significant results of HC-exos on the skin cells in 2D culturing (Fig. 4a-c), its proliferative effect on the three skin cells within the scaffold was analyzed by bioprinting and incubating at 37 °C, followed by visualization with Calcein staining under fluorescence microscopy. Results demonstrate (Fig. 5c,e,g) that the number of cells in the scaffold was relatively higher for the HC-exos@GECM on Day 7 and Day 14, for all three cells. Additionally, the results were quantitatively verified by CCK-8 analysis, showing that the cell proliferation rate was significantly increased for HC-exos@GECM compared to the control (Fig. 5d,f,h), consistent with our previous CCK-8 experiment in 2D culture (Fig. 4a,b,c). Based on the above results, we concluded HC-exos-supplemented bio-ink is highly biocompatible with the three skin cells and beneficial in inducing proliferative effects in a 3D culturing environment. Thereafter, a hemolysis assay was performed with mouse RBC to validate the biocompatibility of the HC-exos@GECM, Org, and Org@HC-exos (3D printed skin organoid with HC-exos in bioink), deploying Triton-X as a positive control and PBS as a negative control. Results indicate that all the above groups induced hemolysis of less than 1 %, proving it highly bio-compatible (Fig. 5i,j).

Overall, all the bio-printed construct was considered safe for implantation in a mouse model for further experimentation.

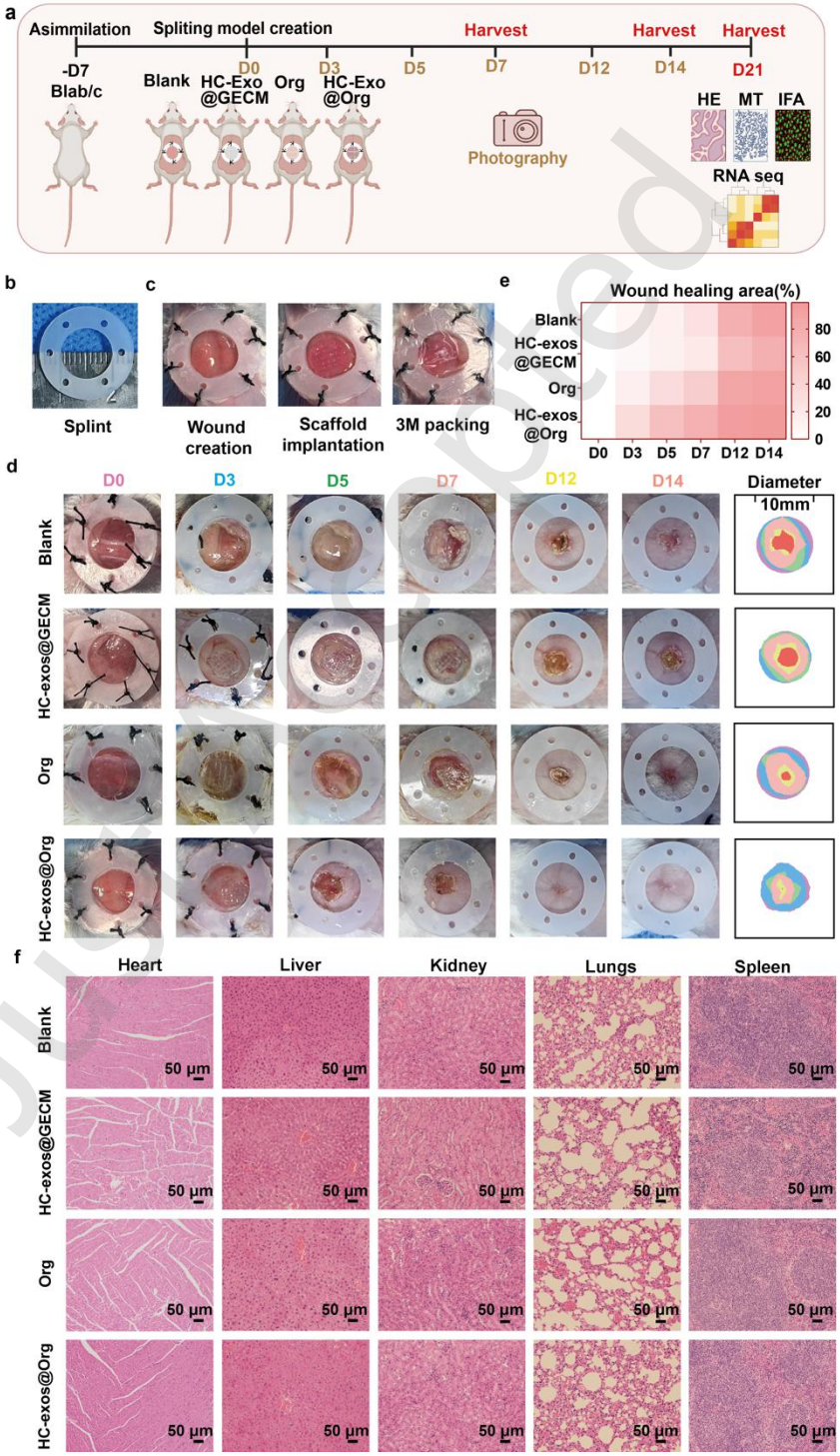

Fig. 6. Evaluation of wound healing effects of 3D printed skin organoid with HC-exos in bio-ink following in vivo implantation. a) Schematic representation of animal experimentation workflow and tissue collection. b) Visual representation of splint size and its c) fixation on the wound, scaffold implantation, followed by 3M packing. d) Digital photography illustrating flow chart of different time points from Day 0 to Day 14 with respective simulation charts. e) Wound healing area in different groups quantitatively (n = 6). f) H&E imaging of the major organs from animal models from different groups collected on Day 14 (scale bar, 50 μm).

2.4 Efficacy of wound healing by 3D printed skin organoid with HC-exos in bio-ink in full-thickness mouse model

To further verify the efficacy of the skin organoid in vivo, we created a full-thickness wound of 10 mm and fixed it with a silicone splint of equal size on the dorsum, as shown in Fig. 6b. In mice, healing mostly takes place through contraction[37]. To mimic skin healing as in humans through granulation and re-epithelization and prevent wound contraction, an excisional wound model with splinting was created as illustrated and randomly distributed into different treatment groups for transplantation of the constructs (Fig. 6a,c). Gross wound healing was digitally photographed at different time periods. While comparing the wound healing efficiency, HC-exos@Org showed a significant wound healing effect with no remaining scab on Day 14 (Fig. 6d). Statistical analysis shows the percentage of wound area changed from 100 % to 1 % on average for the HC-exos@Org group, which was much expedited compared to the other three groups, verifying its superior capability (Fig. 6e). As different toxic reagents were used for the fabrication of ink, improper handling may lead to systemic toxicity and organ failure. To confirm the biocompatibility and safety of our constructs in vivo, histopathological staining of major organs such as heart, liver, spleen, kidney, and lung was performed (Fig. 6f), which reveals no abnormal presentation in any of the treatment groups compared to the blank group, validating the organoids for in vivo application and potentially favorable for future clinical translation.

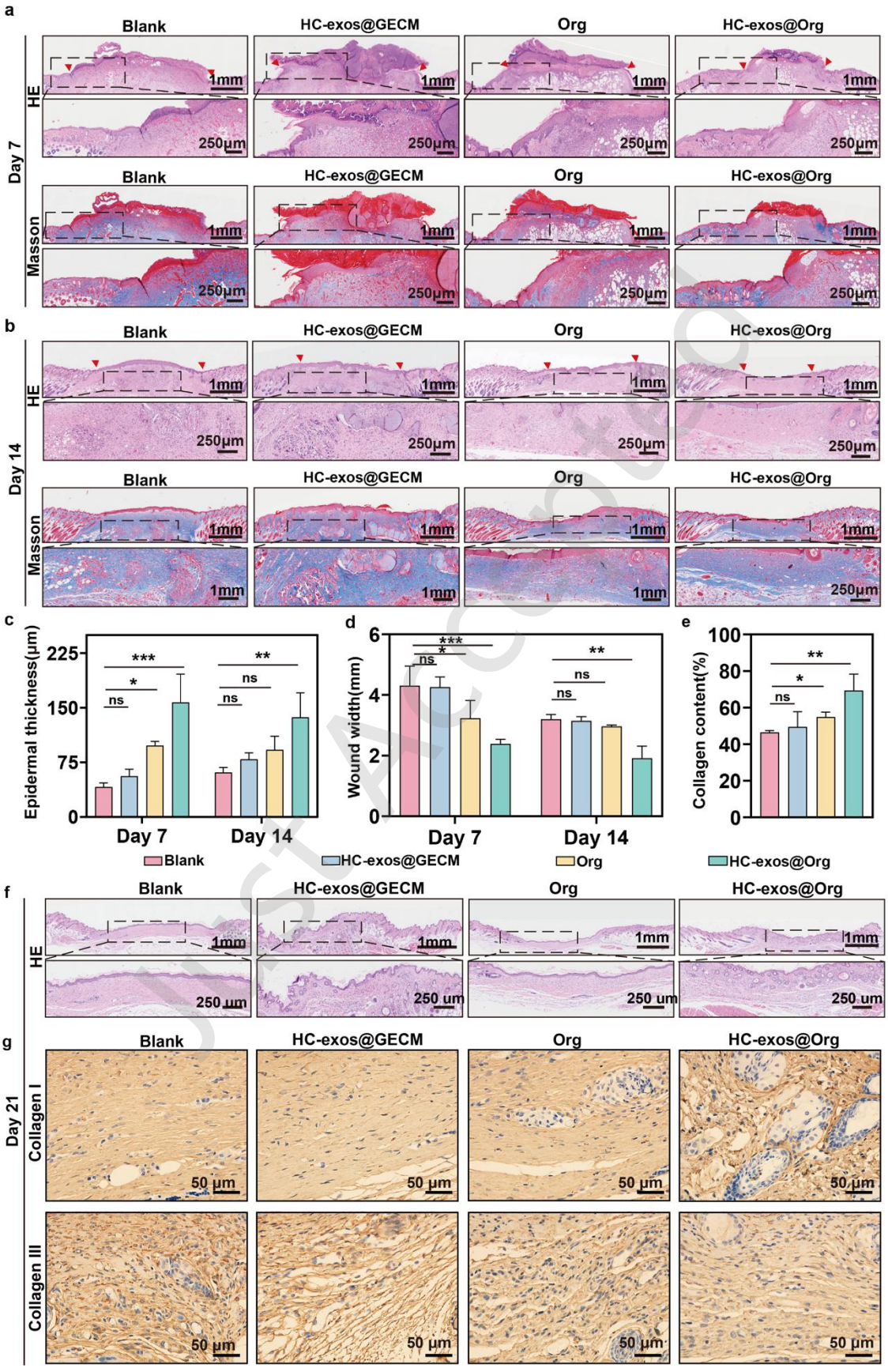

Fig. 7. Histological staining and analysis of skin samples from different treatment groups. a) Hematoxylin and eosin (HE) staining and Masson's Trichome staining on Day 7 (top scale bar, 1 mm), the black dotted area is magnified below (scale bar, 250 μm), and inverted red triangles represent the region of re-epithelization. b) HE staining and Masson's Trichome staining on Day 14. Quantitative analysis of c) epidermal thickness and d) wound width of the tissue on Day 7 and Day 14 (n = 4). e) Collagen content of the tissue on Day 14 (n = 4). Data reported was mean ± standard deviation (*,$p \leq 0.05$; **,$p \leq 0.01$; ***,$p \leq 0.001$, ns: not statistically significant). f) Slide staining with HE for evaluation of hair follicles (scale bar, 1 mm), magnified image within the black dotted lines (scale bar, 250 μm), and g) immunohistochemical staining by type 1 collagen (Collagen I) and type 3 collagen (Collagen III) on Day 21 (scale bar, 50 μm).

To elucidate microscopic changes elicited by different treatments, histopathological analysis on skin samples from each group on Day 7 and Day 14 was performed via hematoxylin and eosin (HE) and Masson staining. The stains reveal complete re-epithelization of the wound region in the HC-exos@Org group on Day 7, whereas HC-exos@GECM and Org groups were mainly covered with crust with incomplete re-epithelization, with the least in the control group (Fig. 7a,b). Epidermal thickness on Day 7 and Day 14 was also significantly thicker in the HC-exos@Org (Fig. 7a-c). Similarly, staining results illustrate wound width to be relatively smaller in the HC-exos@Org group compared to the other groups, both qualitatively and quantitatively. Masson trichome staining also reveals HC-exos@Org exhibited relatively more organized collagen fibers arrangement, compared to other groups (Fig. 7b). The staining also revealed collagen content of the tissue was 79% in HC-exos@Org treatment, while 56.9 %, 61 % and 49 % in Org, HC-exos@GECM, and control, respectively (Fig. 7b,e). In the remodeling phase of wound healing, regeneration of skin appendages poses a significant challenge due to the formation of scar. To investigate whether microtissue can have an impact on the regeneration of hair follicles, we performed H&E staining for the tissue samples on Day 21. Our findings demonstrate that both HC-exos@GECM and HC-exos@Org groups contained relatively more hair follicles, with the HC-exos@Org wound region having the most hair follicles (Fig. 7f), exhibiting its potential in hair follicle regeneration. Se has been reported to substantiate the number of hair follicles, eventually increasing hair density in an androgenetic alopecia mouse model in previous studies[21].

In the process of wound healing, remodeling of collagen types is essential in the formation of normal skin and in preventing scarring. Type 3 collagen (Collagen III) is formed in the early stages mainly expressed in the scar tissue which slowly transitions into type 1 collagen (Collagen I) with maturation of the wound. To examine the effects of different treatments on scarring, wound samples were subjected to immunohistochemistry, revealing that type 1 collagen (Collagen I) was highly expressed in HC-exos@Org aided healing, while type 3 collagen (Collagen III) was relatively lower compared to other groups (Fig. 7g). Given findings demonstrate that HC-exos@Org potentially poses significant implications in accelerated wound healing in the proliferative phase, followed by scar remodeling in later stages.

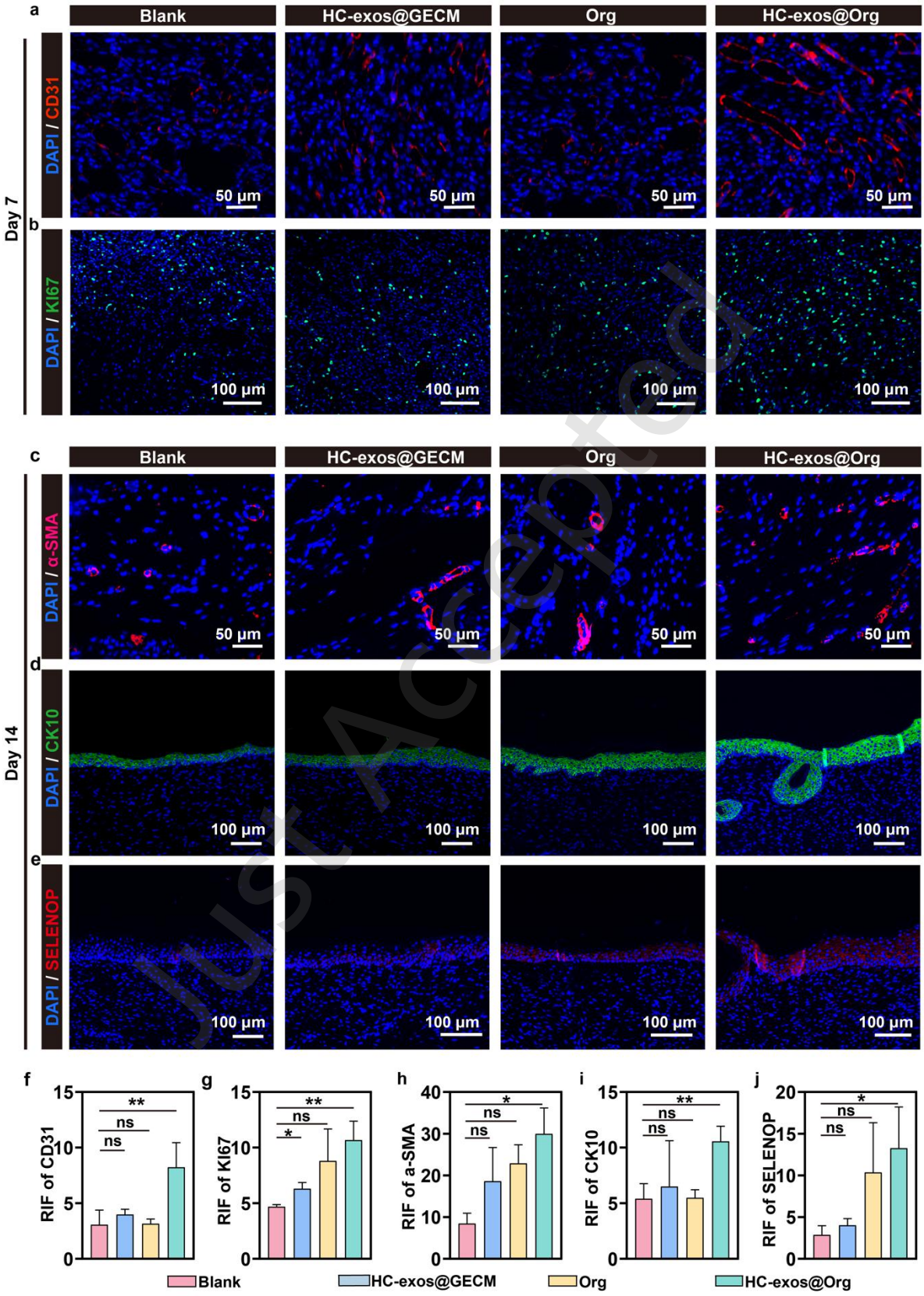

Fig. 8. Immunofluorescence staining of the wound tissue samples. Staining of the skin sample slides with a) CD31 (scale bar, 50 μm), b) KI67 (scale bar, 100 μm) on day 7, c) α -SMA (scale bar, 50 μm), d) CK10 (scale bar, 100 μm), and e) SELENOP (scale bar, 100 μm) on day 14. Quantitative analysis of relative intensity of fluorescence (RIF) of f) CD31, g) KI67, h) α - SMA, i) CK10, and j) SELENOP (n = 4). Data reported was mean ± standard deviation (*,$p \leq 0.05$; **,$p \leq 0.01$; ***,$p \leq 0.001$, ns: not statistically significant).

To navigate the expression of proteins essential for cutaneous regeneration, tissue samples underwent immunofluorescence staining. Cluster of differentiation 31 (CD31) is a transmembrane protein, expressed during neo-vascularization of wound areas for perfusion in early stages of healing. Our results demonstrated a significant increase in fluorescence intensity in HC-exos@Org group, exhibiting its efficiency in angiogenesis on Day 7 (Fig. 8a,f). Similarly, on Day 14, alpha-smooth muscle actin (α-SMA) displayed to be significantly expressed in HC-exos@Org group but was insignificant in other groups, compared to the blank (Fig. 8c,e). These findings prove HC-exos@Org enhances angiogenesis not only in early stages of proliferation, but also in late stages. Furthermore, the data reveal the expression of nuclear protein Kiel 67 antigen (KI67), which is essential in cell proliferation and expressed in dividing cells, to be highly significant in HC-exos@Org group and HC-exos@GECM group (Fig. 8b,g), showing its efficacy in enhancing, proliferation of cells within the wound, that is essential in tissue reformation and vascularization actively. A similar trend was observed for staining of cytokeratin-10 (CK-10), a marker of keratinocyte differentiation, crucial in the maturation of the epidermis. It supports the fact that HC-exos@Org aids in the regeneration of epidermis (Fig. 8d,i). SELENOP staining also showed a similar pattern, with HC-exos@Org group showing the highest fluorescence intensity in epidermal and dermal regions and quantitatively (Fig. 8e,j) supporting the finding that HC-exos@Org can enhance the expression of antioxidant protein in vivo.

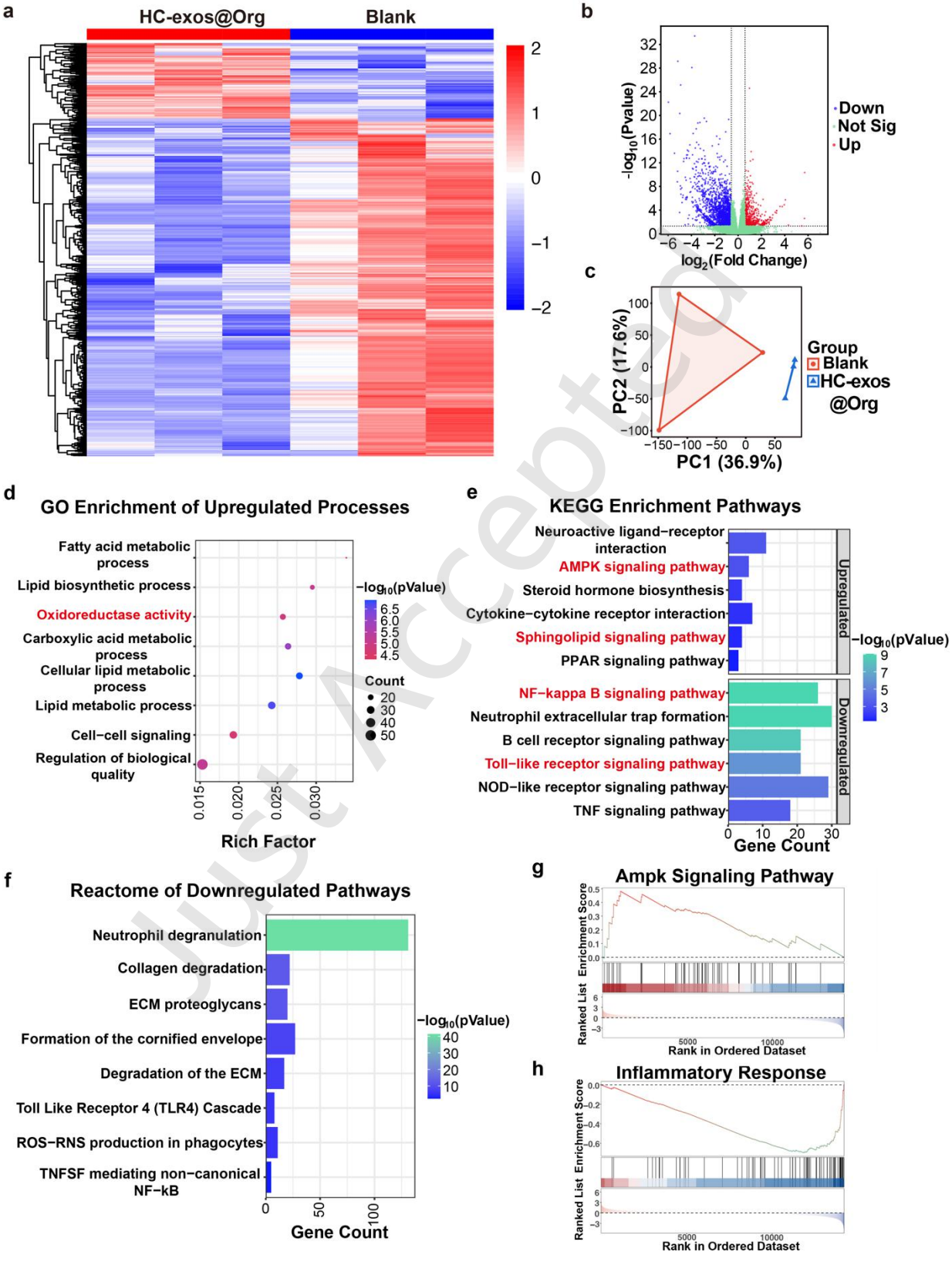

Fig. 9. Transcriptomic analysis of wound healing induced by HC-exos@Org. a) Heatmap of differentially expressed genes in wound skin samples collected from control and HC-exos@Org groups. b) Volcano plot showing the expression of upregulated and downregulated genes. c) Principal component analysis (PCA) of the genes in the two groups. d) GO enrichment analysis of upregulated biological processes e) KEGG enrichment analysis of upregulated and downregulated pathways. f) Reactome of downregulated pathways. GESA analysis of gene sets related to g) AMPK signaling pathway and h) inflammation response signaling pathway.

2.5 Mechanism of accelerated skin regeneration via HC-exos@Org in vivo

To further illustrate the molecular mechanism of HC-exos@Org in wound healing in vivo, we performed transcriptomic analysis of wound tissue samples from blank and the treatment group. Notably, HC-exos@Org exhibited a significant difference in differentially expressed genes with upregulation of 659 genes and downregulation of 2061 genes, as demonstrated in the heatmap and volcano plot (Fig. 9a-b). Principal component analysis (PCA) shows that the genes were distinctly distributed between blank and HC-exos@Org (Fig. 9c). Intriguingly, gene ontology (GO) enrichment analysis for biological processes showed significant enrichment of oxidoreductase activity (Fig. 9d). It supports the fact that HC-exos@Org could activate oxidation-reduction relevant genes and proteins consistent with wound tissue staining findings (Fig. 8e,j). Furthermore, Kyoto Encyclopedia of genes and genomes (KEGG) shows enrichment of pathways such as AMPK (AMP-activated protein kinase) signaling pathway, cytokine-cytokine receptor interaction, PPAR signaling pathway, and Sphingolipid signaling pathway, which are essential in tissue regeneration. Literature also reports sphingolipid signaling pathway is critical for cellular functions such as cell movement, synthesis, and transmission of signaling proteins[31]. Similarly, HC-exos@Org group also downregulated different pro-inflammatory pathways such as nuclear factor kappa-B (NFKB), toll-like receptor, and NOD-like receptor signaling pathways (Fig. 9e), which inhibit the healing process. The reactome graph shows downregulation of different pathways, such as neutrophil degranulation, collagen degradation, and degradation of the ECM, which are essential in wound healing and prevention of fibrotic scars (Fig. 9f). Gene set enrichment analysis (GESA) further verified a modest upregulation of the AMPK-related gene set in HC-exos@Org (Fig. 9g), while downregulation of the gene set

related to the inflammatory response pathway (Fig. 9h). From the above results overall, we can conclude that exosome derived from hepatic cells show promising effects on empowering the skin organoid that can be leveraged for the acceleration of relatively complex full-thickness wound healing.

3. Conclusion

Our study established remarkable regenerative effects of healthy hepatic cells derived seretomes and HC-exos on skin cells, mainly via proliferation, genetic regulation, antioxidation, and angiogenesis. Accounting for the remarkable regenerative impact on the skin cells, we approached the design and generated a skin organoid scaffold bio-printed with cells such as keratinocytes, fibroblasts, and endothelial cells, laden in Gelma-ECM hydrogel containing HC-exos mimicking native skin. The construct after addition of the HC-exos orchestrated significant effects such as anti-oxidation, upregulation of regenerative cellular processes, and regulation of signaling pathways, endowing efficient tissue development in the wound healing micro-environment, presenting as a promising avenue for the management of full-thickness large-area skin injuries. With its excellent biocompatibility and efficacy, it has a high scope in bench-to-bed translation.

Studies have identified HC-exos as a rich source of organic SELENOP that exhibits upregulation of various glutathione-related genes and proteins, with low immunogenicity and high bioavailability[19]. Therefore, its supplementation is crucial for tissue regeneration. Our findings confirmed HC-exos can amplify the regenerative capability of the skin cells via upregulation of cellular mitotic activity, motility, expression of antioxidant molecules such as GXP-4 and SELENOP, and improve angiogenesis, which are essential in the promotion of wound healing[34]. These results may contribute some insights into future research on exosomes-mediated ‘Liver-Skin’ axis for management of different dermatological pathologies. Concurrently, the bio-constructs containing HC-exos can also boost up collagen transformation eventually preventing scarring. Our findings highlight the potential for future research on managing hair-related disorders through synergism of HC-exos with other innovative platforms. For example, integrating microneedles with hepatic exosomes could target specific skin layers to

treat recalcitrant conditions related to antioxidation, hair follicle regeneration, and scar remodeling with minimal invasion and greater convenience[38]. Additionally, the microtissue exhibited upregulation of AMPK signaling pathways. Moderate activation of AMPK in keratinocytes is known to benefit normal wound healing[39] and the regeneration of aging or diabetic wounds[40], opening exciting possibilities for future research in treating inflammation related pathological conditions in dermatology and also in other systems.

4. Methods

Preparation of condition medium (CM)

Transformed human liver epithelial cells (THLE-2) were cultured in THLE-specific medium (Procell, China), 10 % fetal bovine serum (FBS) supplemented by 1 % penicillin and streptomycin. Upon confluence of 80 %, the cells were washed three times with sterile PBS, then cultured in complete medium supplemented with 5 % exosome-free FBS for 48 hours. The resultant supernatant from the culture medium underwent a series of refrigerated centrifugation (Thermo-Scientific, USA) at 300 g for 10 minutes, 2000 g for 20 minutes, followed by 10,000 g for 30 minutes to remove cell debris. After filtering through 0.22 μm (Millipore Sigma, USA). Hepatic conditioned medium (CM) was individually co-cultured with the three skin cells to explore their proliferation rate, genetic regulation, and angiogenic effect.

HC-exos isolation

HC-exos were isolated from CM of THLE-2 cells after ultracentrifuged (Optima XPN-100, Beckman Coulter, USA) at 100,000 g for 120 minutes. The exosome pellet, which was washed with precooled PBS and ultracentrifuged again to acquire pure exosomes that was stored at -80 °C.

Characterization of HC-exos

Isolated HC-exos were subjected to bicinchoninic acid (BCA) assay for protein concentration quantification and for western blotting with exosome-specific surface markers CD 63 and CD 9, and SELENOP was performed. HC-exos sample was dripped on carbon-coated copper 200 μm mesh and underwent negative staining with 2 % phosphotungstic acid (pH ≈ 6) for picturing its

morphology under TEM (JEM-1230, JOEL, Japan). To measure the size distribution of the exosomes in the pellet, Nanoparticle Tracking Analysis (Particle Metrix, ZetaView, Germany) was performed.

HC-exos uptake assay

HC-exos were stained with DIL (Beyotime) and cultured with the skin cells for 24 hours. After washing with PBS, the cell cytoskeleton was stained green with F-actin, and nuclei were stained blue with DAPI. After mounting the plates, they were observed under a confocal laser scanning microscope (Phoenix Optima, Germany).

Cell scratch test

The skin cells were seeded in 2 - well culture inserts (Ibidi, Germany) in 24 - well plates. When cells adhered to the plates, the inserts were removed to create a 500 μm wide gap. The cells were washed with PBS, and culture medium with exosome-deprived serum with or without HC-exos was added to the wells. Images were captured under a bright-field microscope at different time periods, and ImageJ software was used to analyze and compare the results.

Gelma Preparation

Gelma was synthesized by continuously stirring gelatin powder (Sigma-Aldrich, USA) in deionized water until completely dissolved, and methacrylic anhydride was added gradually with stirring. Deionized water was added to stop the reaction. Then, it was dialyzed at 40 °C for 1 week. Lyophilization of the product for three days resulted in a white dry foam that was preserved at -20 °C for further applications.

Decellularization and characterization of skin tissue

Fresh porcine skin was obtained from pigs at a local slaughterhouse. It was decellularized as reported by a previous protocol[41]. Briefly, the epidermis of the tissue was manually discarded from the dermis and was agitated with 0.25 % trypsin solution, 0.1 % SDS in 70 % isopropanol, followed by 1 % Triton X-100 in 70 % isopropanol at 37 °C. Cellular debris and the detergent were removed by thoroughly rinsing with sterile PBS and lyophilized until dry. The decellularized tissue sample and the native tissue were stained with H&E and DAPI to visualize

the presence of cells under bright field and DAPI under immunofluorescence (Olympus BX45 microscope, Japan). DNA quantification was performed through a DNA extraction kit (TIANamp Genomic DNA Kit, Tiangen) for both native skin and ECM using spin columns, and IMPLEM spectrophotometer was used to quantify the DNA concentration, then calculated as ng mg^{-1} of the dried samples. Hydroxyproline quantification kit (Nanjing Jiancheng Bioengineering, China) was used to calculate the collagen content at an absorbance of 550 nm.

Preparation of bio-ink

ECM was solubilized at a concentration of 1mg ml^{-1} pepsin, prepared in diluted hydrochloric acid solution by constant stirring at room temperature. To freshly prepare the ECM solution for bioprinting, pH of those solutions was then adjusted to 7.4 by dropwise addition and stirring with NaOH solution right before mixing with Gelma and the cell suspension.

3D printing of skin organoid

Human keratinocytes (HaCat), human dermal fibroblasts and human umbilical vein endothelial cells (HUVEC) were cultured in DMEM supplemented with 10 % FBS and 1 % Penicillin and Streptomycin at 37 °C in an incubator. Primary cells of passage 4 - 6 were used for experimentation. Keratinocytes were labeled purple with DID (1,1'-Dioctadecyl-3,3,3',3'-Tetramethylindodicarbocyanine Perchlorate), fibroblasts were labeled green with DIO (3,3′-Dioctadecyloxacarbocyanine Perchlorate) and endothelial cells were labeled red with DIL (1,1'-Dioctadecyl-3,3,3',3'-Tetramethylindocarbocyanine Perchlorate). Cell suspension of 10^6 cells ml^{-1} was mixed with sterile GECM bio-ink individually and loaded in their cartridges, and was levelerazed for printing of the 3D organoid scaffolds. Bioprinting parameters were as follows fiber thickness: 0.15 mm, extrusion pressure: 0.05 MPa, printing speed: 5 mm s^{-1}, temperature of cartridges: 20 °C – 25 °C and temperature of printing plane: 10 °C. Endothelial cell layer was initially bio-printed followed by fibroblast layer in between and keratinocyte layer at the top. The organoid was subjected with crosslinking with 405 nm UV light for 10 seconds then view under confocal laser scanning microscope for observing spatial distribution of each type of cell within their layers.

Cell compatibility analysis

The bio-printed scaffolds with or without exosomes were stained with Calcein (Beyotime) according to the instructions in the user's manual to analyze the biocompatibility and proliferation in a 3D environment. Calcein stained living cells green while unviable cells appeared red under an immunofluorescence microscope, which was photographed on Day 1, Day 3, and Day 7.

Animal experiment

All animal experiments were conducted as per approved protocol for animal care and laboratory animals by the committee of animal care of Tongji University, Shanghai (Ethical approval number - TJAA15125101) and animal license number – SYXK (Hu) 2020-0002. 5-6 weeks old BLAB/c female mice were purchased and fostered in a controlled 12 - hours alternating day and night cycle with unlimited food and water access for a week. The mice were anesthetized under inhaled isoflurane at 10 % and maintained at 5 % to remove dorsal hair. After sterilizing the hairless area, a sterile 10mm punch biopsy was used to create a full-thickness wound, and a sterile splint was sutured to fix around it to prevent wound healing by contraction. The mice were then divided into four groups such as 1) wound without any scaffold (blank), 2) HC-exos@GECM group, 3) Org group, and 4) HC-exos@Org group for transplantation. Finally, packing was done with sterile 3M Tegaderm and photographed at different time intervals.

Histological analysis

Skin samples were collected and fixed in 4 % paraformaldehyde for 24 hours. Then, it underwent dehydration through an alcohol series followed by paraffin embedding. The tissues were then sliced at a thickness of 5 μm. After deparaffinization, the skin slides were stained with Hematoxylin and Eosin (HE) and Masson's trichome stain, followed by scanning via Slideview VS200 (Olympus, Japan). The slides underwent immunohistochemistry with specific antibodies and were observed under a BX45 fluorescence microscope (Olympus, Japan) under bright field and fluorescence emission.

Statistical analysis

GraphPad Prism (version 8.0) was used for the analyzing statistical data. All the experiments were performed at least in triplicate. Student's *t*-test (two-tailed), was used for analyzing

significance pairwise. For multiple groups comparison, one-way ANOVA was performed. *$p<$ 0.05, **$p<$ 0.01 and ***$p<$ 0.001 was considered as statistically significant. All data were represented as mean ± standard deviation.

Data Availability

The data of this study are available from the corresponding author upon reasonable request.

Competing Interests

Authors declare no competing interests.

Acknowledgment

This work was supported by grants from the National Natural Science Foundation of China (82072258, 82373482) and Shanghai Natural Science Foundation(24ZR1450100).

Resources

[i] **https://www.who.int/en/news-room/fact-sheets/detail/burns**

References

[1] Zhou, X. J.;Brown, B. A.;Siegel, A. P.;El Masry, M. S.;Zeng, X. Y.;Song, W. R.;Das, A.;Khandelwal, P.;Clark, A.;Singh, K.;Guda, P. R.;Gorain, M.;Timsina, L.;Xuan, Y.;Jacobson, S. C.;Novotny, M. V.;Roy, S.;Agarwal, M.;Lee, R. J.;Sen, C. K.;Clemmer, D. E.; Ghatak, S. Exosome-Mediated Crosstalk between Keratinocytes and Macrophages in Cutaneous Wound Healing. *Acs Nano* **2020**, *14*, 12732-12748.

[2] Mauro, T.; Bikle, D. Skin and bone crosstalk during aging. *Nat Aging* **2022**, *2*, 874-875.

[3] Pena, O. A.; Martin, P. Cellular and molecular mechanisms of skin wound healing. *Nat Rev Mol Cell Biol* **2024**, 10.1038/s41580-024-00715-1.

[4] Meara, J. G.;Leather, A. J.;Hagander, L.;Alkire, B. C.;Alonso, N.;Ameh, E. A.;Bickler, S. W.;Conteh, L.;Dare, A. J.;Davies, J.;Merisier, E. D.;El-Halabi, S.;Farmer, P. E.;Gawande, A.;Gillies, R.;Greenberg, S. L.;Grimes, C. E.;Gruen, R. L.;Ismail, E. A.;Kamara, T. B.;Lavy, C.;Lundeg, G.;Mkandawire, N. C.;Raykar, N. P.;Riesel, J. N.;Rodas, E.;Rose, J.;Roy, N.;Shrime, M. G.;Sullivan, R.;Verguet, S.;Watters, D.;Weiser, T. G.;Wilson, I. H.;Yamey, G.; Yip, W. Global Surgery 2030: evidence and solutions for achieving health, welfare, and economic development. *Lancet* **2015**, *386*, 569-624.

[5] Herskovitz, I.;Hughes, O. B.;Macquhae, F.;Rakosi, A.; Kirsner, R. Epidermal skin grafting. *Int Wound J* **2016**, *13 Suppl 3*, 52-56.

[6] Yan, J.;Ye, Z.;Lu, Y.;Yuan, Y.;Wang, X.;Yan, T.;Yin, J.; Wang, Y. 3D bioprinting lobule-like hepatorganoids with induced vascularization for orthotopic implantation. *Mater Today Bio* **2025**, *31*, 101515.
[7] Kim, B. S.;Gao, G.;Kim, J. Y.; Cho, D. W. 3D Cell Printing of Perfusable Vascularized Human Skin Equivalent Composed of Epidermis, Dermis, and Hypodermis for Better Structural Recapitulation of Native Skin. *Adv Healthc Mater* **2019**, *8*, e1801019.
[8] Jorgensen, A. M.;Gorkun, A.;Mahajan, N.;Willson, K.;Clouse, C.;Jeong, C. G.;Varkey, M.;Wu, M.;Walker, S. J.;Molnar, J. A.;Murphy, S. V.;Lee, S. J.;Yoo, J. J.;Soker, S.; Atala, A. Multicellular bioprinted skin facilitates human-like skin architecture in vivo. *Sci Transl Med* **2023**, *15*, eadf7547.
[9] Liu, X.;Michael, S.;Bharti, K.;Ferrer, M.; Song, M. J. A biofabricated vascularized skin model of atopic dermatitis for preclinical studies. *Biofabrication* **2020**, *12*.
[10] Zhang, T.;Sheng, S.;Cai, W.;Yang, H.;Li, J.;Niu, L.;Chen, W.;Zhang, X.;Zhou, Q.;Gao, C.;Li, Z.;Zhang, Y.;Wang, G.;Shen, H.;Zhang, H.;Hu, Y.;Yin, Z.;Chen, X.;Liu, Y.;Cui, J.; Su, J. 3-D bioprinted human-derived skin organoids accelerate full-thickness skin defects repair. *Bioact Mater* **2024**, *42*, 257-269.
[11] Dutta, S. D.;An, J. M.;Hexiu, J.;Randhawa, A.;Ganguly, K.;Patil, T. V.;Thambi, T.;Kim, J.;Lee, Y.-k.; Lim, K.-T. 3D bioprinting of engineered exosomes secreted from M2-polarized macrophages through immunomodulatory biomaterial promotes in vivo wound healing and angiogenesis. *Bioact Mater* **2025**, *45*, 345-362.
[12] Wang, T. C.;Li, W. T.;Zhang, Y. X.;Xu, X.;Qiang, L.;Miao, W. Q.;Yue, X. K.;Jiao, X.;Zhou, X. H.;Ma, Z. J.;Li, S.;Ding, M. L.;Zhu, J. F.;Yang, C.;Wang, H.;Li, T.;Sun, X.; Wang, J. W. Bioprinted constructs that simulate nerve-bone crosstalk to improve microenvironment for bone repair. *Bioact Mater* **2023**, *27*, 377-393.
[13] Jin, Y.;Zhang, J.;Chen, X.;Li, F.;Xue, T.;Yi, K.;Xu, Y.;Wang, H.;Lao, Y. H.;Chan, H. F.;Shao, D.;Li, M.; Tao, Y. 3D printing incorporating gold nanozymes with mesenchymal stem cell-derived hepatic spheroids for acute liver failure treatment. *Biomaterials* **2024**, *315*, 122895.
[14] Michalopoulos, G. K.; Bhushan, B. Liver regeneration: biological and pathological mechanisms and implications. *Nat Rev Gastroenterol Hepatol* **2021**, *18*, 40-55.
[15] Sung, S.;Kim, J.; Jung, Y. Liver-Derived Exosomes and Their Implications in Liver Pathobiology. *International Journal of Molecular Sciences* **2018**, *19*.
[16] Nojima, H.;Freeman, C. M.;Schuster, R. M.;Japtok, L.;Kleuser, B.;Edwards, M. J.;Gulbins, E.; Lentsch, A. B. Hepatocyte exosomes mediate liver repair and regeneration via sphingosine-1-phosphate. *J Hepatol* **2016**, *64*, 60-68.
[17] Bai, S.;Zhang, M.;Tang, S.;Li, M.;Wu, R.;Wan, S.;Chen, L.;Wei, X.; Feng, S. Effects and Impact of Selenium on Human Health, A Review. *Molecules* **2024**, *30*.
[18] Ye, R. H.;Huang, J. Q.;Wang, Z. X.;Chen, Y. X.; Dong, Y. L. The Role and Mechanism of Essential Selenoproteins for Homeostasis. *Antioxidants-Basel* **2022**, *11*.
[19] Jin, Y.;Chung, Y. W.;Jung, M. K.;Lee, J. H.;Ko, K. Y.;Jang, J. K.;Ham, M.;Kang, H.;Pack, C. G.;Mihara, H.; Kim, I. Y. Apolipoprotein E-mediated regulation of selenoprotein P transportation via exosomes. *Cell Mol Life Sci* **2020**, *77*, 2367-2386.
[20] Xie, B.;Zeng, D. L.;Yang, M. J.;Tang, Z. Y.;He, L. Z.; Chen, T. F. Translational Selenium Nanoparticles to Attenuate Allergic Dermatitis through Nrf2-Keap1-Driven Activation of Selenoproteins. *Acs Nano* **2023**, *17*, 14053-14068.

[21] Jing, S.;Liu, Y.;Wang, B.;Zhou, H.;Zhang, H.;Siwakoti, P.;Qu, X.;Ye, P.;He, Y.;Kumeria, T.; Ye, Q. Microneedle-mediated hypoxic extracellular vesicle-encapsulated selenium nanoparticles delivery to treat androgenetic alopecia. *J Control Release* **2025**, 10.1016/j.jconrel.2025.113597, 113597.
[22] Heo, J. S. Selenium-Stimulated Exosomes Enhance Wound Healing by Modulating Inflammation and Angiogenesis. *Int J Mol Sci* **2022**, *23*.
[23] Nobili, V. Liver-skin axis: a new view or viewed already? *Br J Dermatol* **2018**, *179*, 6.
[24] Nakajima, H.;Nakajima, K.;Takaishi, M.;Ohko, K.;Serada, S.;Fujimoto, M.;Naka, T.; Sano, S. The Skin-Liver Axis Modulates the Psoriasiform Phenotype and Involves Leucine-Rich alpha-2 Glycoprotein. *J Immunol* **2021**, *206*, 1469-1477.
[25] Marani, M.;Madan, V.;Le, T. K.;Deng, J.;Lee, K. K.;Ma, E. Z.; Kwatra, S. G. Dysregulation of the Skin-Liver Axis in Prurigo Nodularis: An Integrated Genomic, Transcriptomic, and Population-Based Analysis. *Genes (Basel)* **2024**, *15*.
[26] Guo, X. L.;Wang, Y. D.;Liu, Y. J.;Chu, L.;Zhu, H.;Hu, Y.;Wu, R. Y.;Xie, H. Y.;Yu, J.;Li, S. P.;Xiong, C. Y.;Li, R. Y.;Ke, F.;Chen, L.;Chen, G. Q.;Chen, L.;Bai, F.;Enver, T.;Li, G. H.;Li, H. F.; Hong, D. L. Fetal hepatocytes protect the HSPC genome via fetuin-A. *Nature* **2025**, *637*, 402-411.
[27] Liu, J.;Dou, G.;Zhao, W.;Hu, J.;Jiang, Z.;Wang, W.;Wang, H.;Liu, S.;Jin, Y.;Zhao, Y.;Chen, Q.; Li, B. Exosomes derived from impaired liver aggravate alveolar bone loss via shuttle of Fasn in type 2 diabetes mellitus. *Bioact Mater* **2024**, *33*, 85-99.
[28] Ye, L.;Li, S.;Bi, G.;Li, B.;Cai, Z.;Jin, M.;Zhang, Y.;Yang, W.;Li, Y.;Li, S.;Hu, W.;Gao, Y.;Pan, M.;Zhou, S.;Zhang, C.;Bi, H.; Peng, Q. Exosomes From Intestinal Epithelial Cells Promote Hepatic Differentiation of Liver Progenitor Cells in Gut-Liver-on-a-Chip Models. *Adv Sci (Weinh)* **2025**, *12*, e17478.
[29] Lu, J. W.;Yang, X. H.;He, C. F.;Chen, Y. Z.;Li, C. S.;Li, S. H.;Chen, Y. W.;Wu, Y. F.;Xiang, Z. H.;Kang, J. W.;Jiang, G. Y.;Wang, C.;Diarra, M. D.;He, R. X.;Feng, G.; Yan, R. J. Rejuvenation of tendon stem/progenitor cells for functional tendon regeneration through platelet-derived exosomes loaded with recombinant Yap1. *Acta Biomaterialia* **2023**, *161*, 80-99.
[30] Cui, Y.;Hong, S.;Xia, Y.;Li, X.;He, X.;Hu, X.;Li, Y.;Wang, X.;Lin, K.; Mao, L. Melatonin Engineering M2 Macrophage-Derived Exosomes Mediate Endoplasmic Reticulum Stress and Immune Reprogramming for Periodontitis Therapy. *Adv Sci (Weinh)* **2023**, 10.1002/advs.202302029, e2302029.
[31] Hla, T.; Dannenberg, A. J. Sphingolipid Signaling in Metabolic Disorders. *Cell Metabolism* **2012**, *16*, 420-434.
[32] Zhang, F.;Li, X.; Wei, Y. Selenium and Selenoproteins in Health. *Biomolecules* **2023**, *13*.
[33] Liang, X.;Xue, Z.;Zheng, Y.;Li, S.;Zhou, L.;Cao, L.; Zou, Y. Selenium supplementation enhanced the expression of selenoproteins in hippocampus and played a neuroprotective role in LPS-induced neuroinflammation. *Int J Biol Macromol* **2023**, *234*, 123740.
[34] Zhao, Y.;Chen, Z.;Xie, S.;Xiao, F.;Hu, Q.; Ju, Z. The emerging role and therapeutical implications of ferroptosis in wound healing. *Burns Trauma* **2025**, *13*, tkae082.
[35] Huang, Z.;Rose, A. H.; Hoffmann, P. R. The role of selenium in inflammation and immunity: from molecular mechanisms to therapeutic opportunities. *Antioxid Redox Signal* **2012**, *16*, 705-743.

[36] Zhou, J.;Jiang, S.;Wang, L.;Lin, K.;Wu, J.;Gui, H.; Gao, Z. Decellularized Adipose Matrix Rejuvenates Photoaged Skin through Immune Microenvironment Modulation. *BME Front* **2025**, *6*, 0166.
[37] Wang, X.;Ge, J.;Tredget, E. E.; Wu, Y. The mouse excisional wound splinting model, including applications for stem cell transplantation. *Nat Protoc* **2013**, *8*, 302-309.
[38] Xu, C.;Wu, F.;Duan, Z.;Rajbanshi, B.;Qi, Y.;Qin, J.;Dai, L.;Liu, C.;Jin, T.;Zhang, B.; Zhang, X. Microneedle-aided nanotherapeutics delivery and nanosensor intervention in advanced tissue regeneration. *J Nanobiotechnology* **2025**, *23*, 330.
[39] Takaya, K.;Okabe, K.;Sakai, S.;Aramaki-Hattori, N.;Asou, T.; Kishi, K. Salicylate induces epithelial actin reorganization via activation of the AMP-activated protein kinase and promotes wound healing and contraction in mice. *Sci Rep* **2024**, *14*, 16442.
[40] Qi, Y.;Rajbanshi, B.;Hao, R.;Dang, Y.;Xu, C.;Lu, W.;Dai, L.;Zhang, B.; Zhang, X. The dual role of PGAM5 in inflammation. *Exp Mol Med* **2025**, *57*, 298-311.
[41] Ventura, R. D.;Padalhin, A. R.;Park, C. M.; Lee, B. T. Enhanced decellularization technique of porcine dermal ECM for tissue engineering applications. *Mat Sci Eng C-Mater* **2019**, *104*.

Electronic Supplementary Material

3D bioprinting of hepatocyte-derived exosome-reinforced skin organoid for efficient skin regeneration

Bhavana Rajbanshi[1], Churong Xu[3], Surendra Shrestha[5], Ruihan Hao[3], Yuxin Qi[3], Zhouyi Duan[3], Ding Ma[3], Qichen Li[3], Fangzheng Cheng[3], Liming Dai[3], Miao Jiang[1], Xiaoling Zhang[3*], Bingjun Zhang[4*], and Jingjun Zhao[1,2*]*

1. Department of Dermatology and Venereology, Tongji Hospital, School of Medicine, Tongji University, Shanghai 200092, China
2. Department of Dermatology, Xinhua Hospital Affiliated to Shanghai Jiao Tong University School of Medicine, Shanghai 200092, China
3. Department of Orthopedics, Xinhua Hospital Affiliated to Shanghai Jiao Tong University School of Medicine, Shanghai 200092, China
4. Suzhou Institute of Biomedical Engineering and Technology, Chinese Academy of Sciences, Suzhou 215163, China
5. Department of Pediatrics, Maria Fareri Children's Hospital at Westchester Medical Center, Valhalla, NY 10595, USA

✉Address correspondence to Jingjun Zhao, zhaojingjun2015@aliyun.com; Bingjun Zhang, smior122@163.com; Xiaoling Zhang, xlzhang@shsmu.edu.cn; Miao Jiang, jiang-miao@126.com

Supporting information to https://doi.org/10.26599/NR.2026.94908759

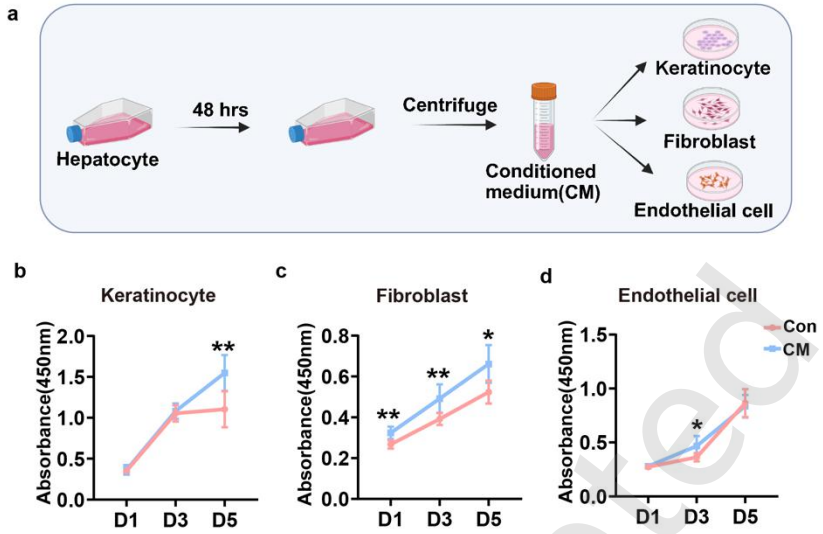

Fig. S1 Effects of conditioned medium (CM) from hepatocytes on proliferation of different skin cells. a) Illustration of workflow for preparation of conditioned medium (CM) from hepatocytes and culturing of skin cells. b,c,d) The proliferation activities of keratinocytes, fibroblasts, and endothelial cells after being cultured for 1, 3, and 5 days (n = 4). Data reported was mean ± standard deviation (*,$p \leq 0.05$; **,$p \leq 0.01$; ***,$p \leq 0.001$ vs. control, ns: not significant).

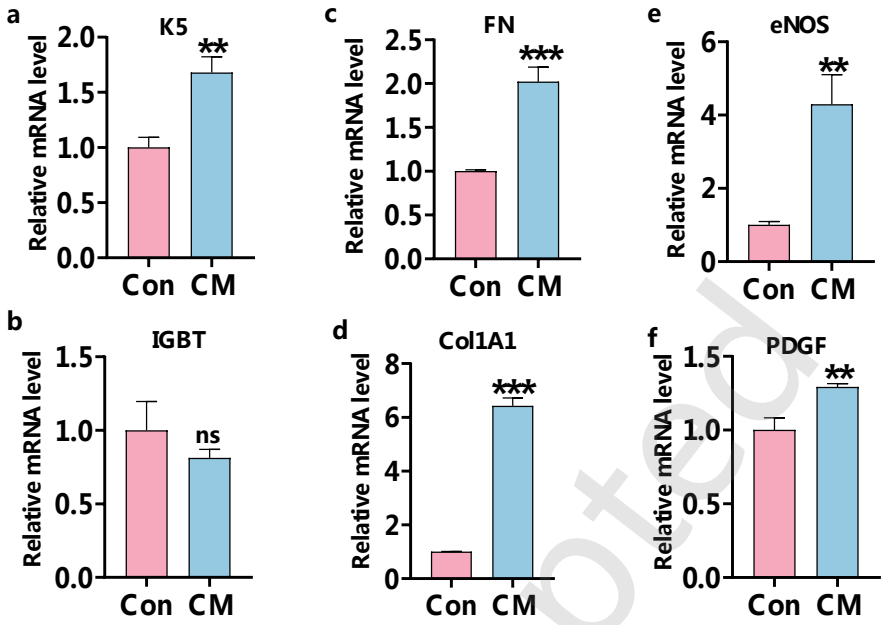

Fig. S2 Effects of conditioned medium (CM) from hepatocytes on Gene expression of different skin cells. Gene expression of a,b) K5 and IGBT in keratinocytes, c,d) FN and Col1A1 in fibroblasts, e,f) eNOS and PDGF in endothelial cells after culturing for 2 days using RT-PCR (n = 9). Data reported was mean ± standard deviation (*,$p \leq 0.05$; **,$p \leq 0.01$; ***,$p \leq 0.001$ vs. control, ns: not significant).

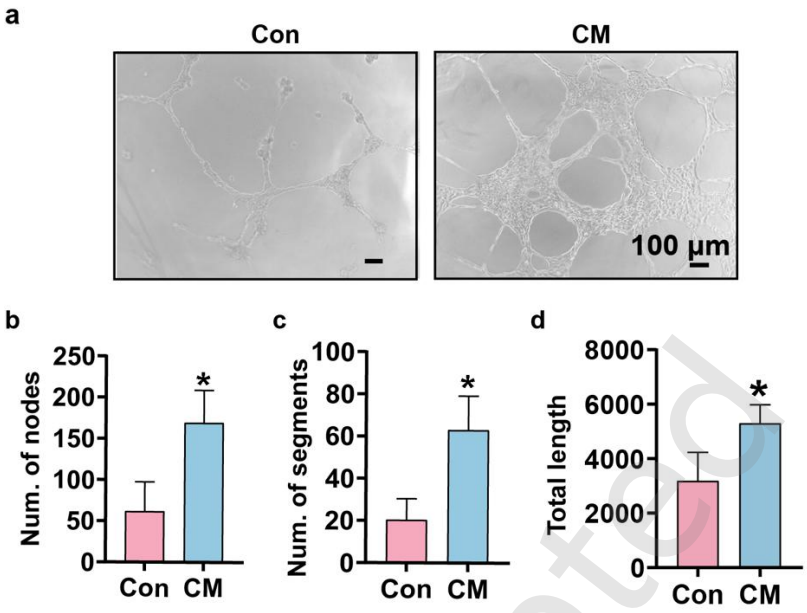

Fig. S3 Effects of conditioned medium (CM) from hepatocytes on angiogenesis**.** a) Angiogenesis images of endothelial cells. b,c,d) Quantitative analysis of the number of nodes, segments and tube length (n = 3). Data reported was mean ± standard deviation (*,$p \leq 0.05$; **,$p \leq 0.01$; ***,$p \leq 0.001$ vs. control, ns: not significant).

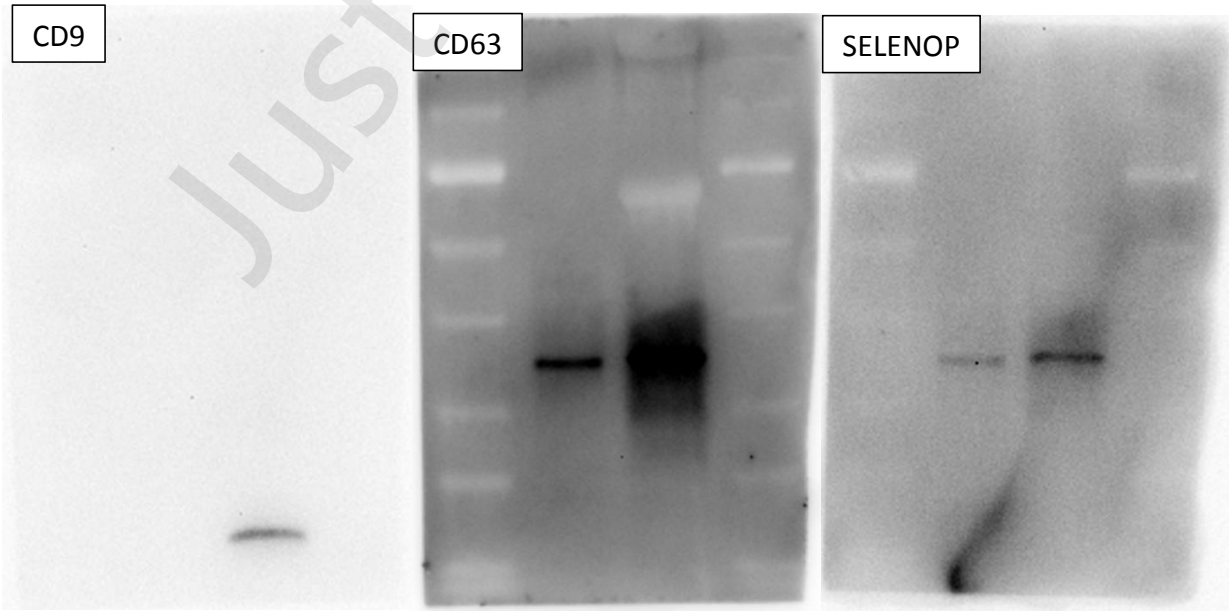

Fig. S4. Western blot of different exosome MARKER proteins CD9, CD63 and SELENOP, respectively.

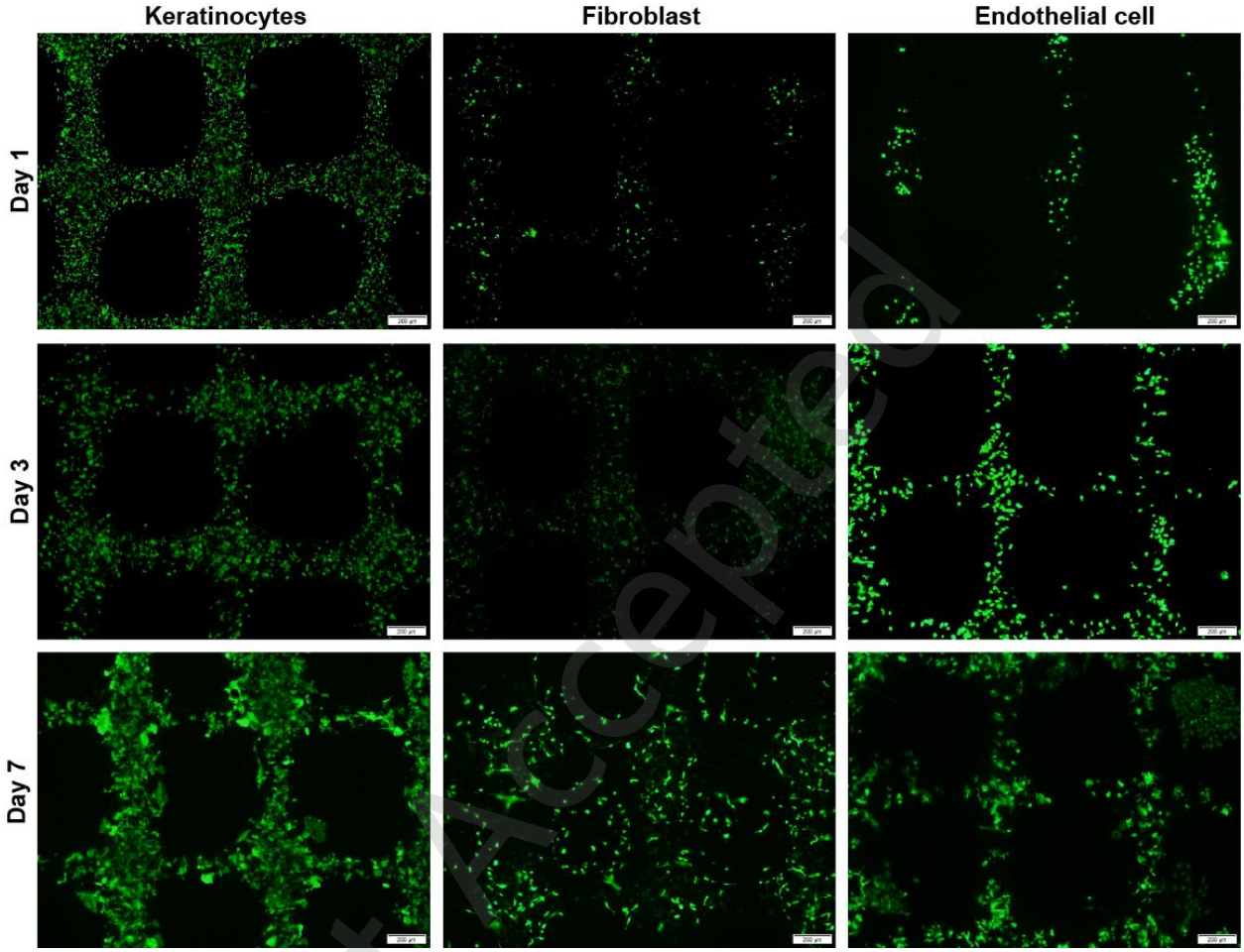

Fig.S5 Biocompatibility of bio ink on three different skin cells on Day 1, Day 3, and Day 7

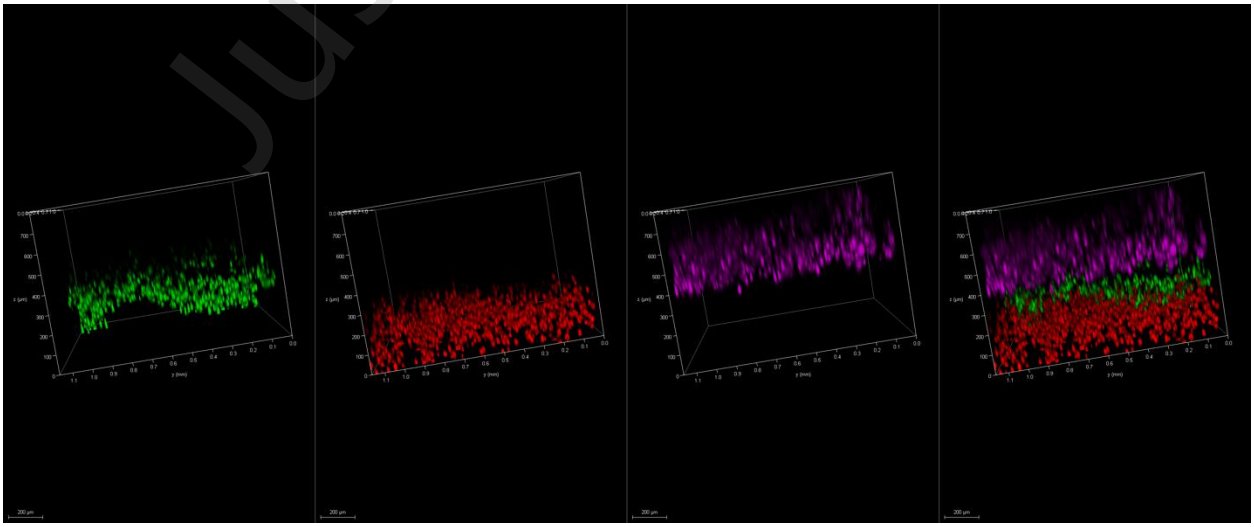

Fig. S6 3D spatial observation of different skin cells stained with cell membrane markers of different colors

Supplementary Table 1
Primer's sequence

Primers	Sequences
Cytokeratin 5 forward	GGCGAGGAATGCAGACTCAG
Cytokeratin 5 Reverse	GTAGCTTCCACTGCTACCTCC
Cytokeratin 15 forward	AGATCGCTACTTACCGCAGC
Cytokeratin 15 Reverse	CCACCTGTCCATCCACTGAC
Fibronectin 1 Forward	TCAGCTTCCTGGCACTTCTG
Fibronectin 1 Reverse	TCTTGTCCTACATTCGGCGG
Collagen 1A1 Forward	AGTGGTTTGGATGGTGCCAA
Collagen 1A1 Reverse	GCACCATCATTTCCACGAGC
GPX2 Forward	CAAGTATGTCCGTCCTGGGG
GPX2 Reverse	TCAGGTAGGCGAAGACAGGA
eNOS Forward	GTGTCCCTCGAACACGAGAC
eNOS Reverse	AGTGGGTCTGAGCAGGAGAT
PDGFb Forward	TCCTGTCTCTCTGCTGCTAC
PDGFb Reverse	CATCAAAGGAGCGGATCGAGT
GAPDH Forward	TCACCAAGTTTGGACACCGT
GAPDH Reverse	ATAGTGGGGCAGGTCCTTCT
GXP4 Forward	TCACCAAGTTTGGACACCGT
GXP4 Reverse	ATAGTGGGGCAGGTCCTTCT

Supplementary Table 2

Antibody	Supplier	Cat no.
CD9	Proteintech	20597-1-AP
CD63	Proteintech	25682-1-AP
SELENOP	AB Clonal	A23647
CD31	Abcam	ab28364
a-SMA	Invitrogen	14-9760-82
KI67	Servicebio	GB151499
Collagen 3	Servicebio	GB111629
Collagen 1	Servicebio	GB11022-3
CK10	AB Clonal	A4669